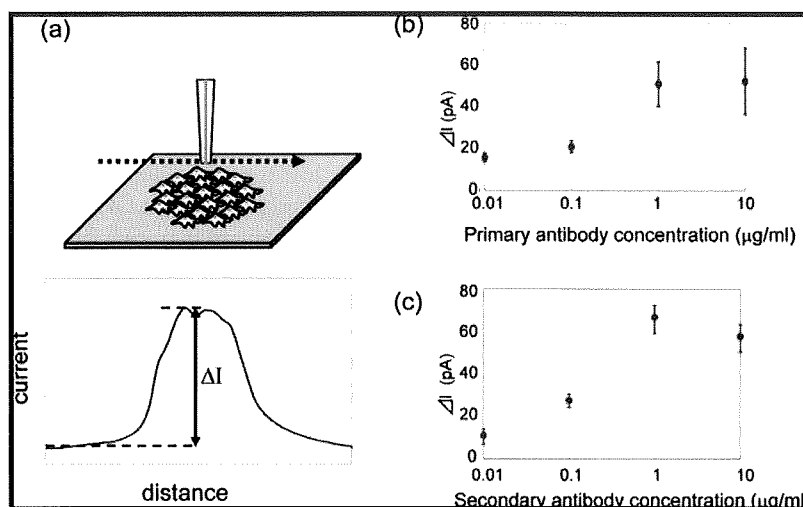


**Figure 1.** Schematic diagrams of EGFR detection using (a) generation-collection mode and (b) feedback mode.



**Figure 2.** Optimization of antibody concentration. (a) Schematic representation of standardization of current  $\Delta I$ . Oxidation current response as a function of the (b) primary antibody concentration (secondary antibody concentration is  $1 \mu\text{g/ml}$ ) and (c) secondary antibody concentration (primary antibody concentration is  $10 \mu\text{g/ml}$ ). The electrode was set at  $20 \mu\text{m}$  above the substrate, and the scan rate was  $10 \mu\text{m/s}$ .

product, which was detected electrochemically at the microelectrode probe of SECM set at  $+0.30 \text{ V vs Ag/AgCl}$  (Figure 1a). In the case of Dp labeling, the potential of the probe was set at  $+0.35 \text{ V vs Ag/AgCl}$  to oxidize  $\text{FcCH}_2\text{OH}$  to  $[\text{FcCH}_2\text{OH}]^+$ , which was reduced again to  $\text{FcCH}_2\text{OH}$  by the Dp-catalyzed reaction at the membrane surface in the presence of NADH. This enzymatic regeneration of  $\text{FcCH}_2\text{OH}$  increased the oxidation current at the probe (Figure 1b).

A disk-type platinum electrode with a  $20 \mu\text{m}$  diameter was used as a SECM microelectrode probe and as a working electrode. Electrochemical current was measured on the basis of a two-electrode configuration using an Ag/AgCl electrode as the reference electrode. The current was amplified with a current amplifier (428, Keithley). Movement of the microelectrode tip was performed by a motor-driven XYZ stage (K701-20RMS, Suruga Seiki) and a stage controller (D70, Suruga Seiki). The details of the SECM system were reported previously.<sup>18</sup>

**Preparation of the Cell-Patterned Substrate.** For the estimation of EGFR expression levels, a flat substrate patterned with approximately 300 cells was fabricated by the PDMS microstenciling method. The microstencil was a  $100 \mu\text{m}$ -thick

PDMS sheet with a  $3 \times 3$  array of  $300 \mu\text{m}$  diameter circles, prepared using a  $\text{CO}_2$  laser beam (Universal Laser Systems, Scottsdale, Arizona). The cells ( $10^6$  cells/mL,  $100 \mu\text{L}$ ) were seeded on a 35 mm dish (Falcon), sealed with the PDMS microstencil, and incubated for 2 h to allow the cells to adhere to the dish. The excess nonadherent cells were then removed by washing with RPMI-1640. After incubation for 1 day in RPMI-1640, the stencil was peeled off from the dish and the SECM measurement was performed (Figure 2a).

## RESULTS AND DISCUSSION

Because the SECM is sensitive to the diffusion and permeation of chemicals, SECM measurements can distinguish whether a chemical reagent is derived from the outside or inside of the cell

- (31) Matsue, T.; Shiku, H.; Yamada, H.; Uchida, I. *J. Phys. Chem.* 1994, 98, 11001–11003.
- (32) Wilburn, J. P.; Wright, D. W.; Cliffel, D. E. *Analyst* 2006, 131, 311–316.
- (33) Sun, P.; Laforge, F. O.; Abeyweera, T. P.; Rotenberg, S. A.; Carpino, J.; Mirkin, M. V. *Proc. Natl. Acad. Sci. U.S.A.* 2008, 105, 443–448.
- (34) Feng, W.; Rotenberg, S. A.; Mirkin, M. V. *Anal. Chem.* 2003, 75, 4148–4154.
- (35) Zhan, W.; Bard, A. J. *Anal. Chem.* 2006, 78, 726–733.

membrane.<sup>19,31–35</sup> Furthermore, real-time monitoring of cell surface phenomena, including endocytosis and exocytosis,<sup>21,36–39</sup> is also possible. In this study, we optimized the concentration of the primary and secondary antibodies for EGFR labeling. We used three types of cells: normal CHO without EGFR, EGFR/CHO expressing EGFR, and A431 originally expressing EGFR with very high density. The current response that originated from ALP-labeled EGFR at the cell membranes was measured with the SECM in a HEPES-based saline solution of pH 9.5. During the measurements, the cells were alive for at least 3 h in the solution, although it is important to consider the toxicity of the enzyme substrate and the product. The results were compared with those from flow cytometry (see Supporting Information).

**Optimization of Antibody Concentration by SECM Measurements.** The binding ability of the ALP antibody to EGFR was estimated from the PAP oxidation current produced by the ALP-catalyzed reaction at the cell surfaces. The PAP oxidation was measured by a single-scan measurement above a circular cell pattern comprising approximately 300 EGFR/CHO cells. Larger oxidation currents were observed when the microelectrode probe scanned over the cell pattern. The peak response, observed at the center of the pattern (Figure 2a), increased as the primary or secondary antibody concentration for ALP labeling of EGFR increased (Figure 2b,c). On the basis of these results, in subsequent measurements, the concentrations of both the primary and secondary antibodies were set at 1  $\mu\text{g/mL}$ .

**Investigation of CHO Cells Using  $\beta$ -Gal or Dp as a Labeling Enzyme with SECM.** We also used  $\beta$ -Gal as an EGFR-labeling enzyme because  $\beta$ -Gal functions in neutral pH. Figure 3 shows the current responses obtained by a single-scan measurement with the SECM substrate generation/tip collection mode for the cell patterns of  $\beta$ -Gal-labeled EGFR/CHO cells and nonlabeled EGFR/CHO cells. The current responses of EGFR/CHO cells were found to be less than 3 pA, which was 1 order of magnitude smaller than that found for ALP-labeled cells. Therefore, we concluded that  $\beta$ -Gal is not suitable for single-cell imaging since single-cell imaging requires a highly active enzyme to detect a small number of EGFRs. However, it should be noted that  $\beta$ -Gal labeling minimized the background current, as evident by the fact that no response was observed for the nonlabeled EGFR/CHO cells. Usually, mammalian cells naturally have no endogenous galactosidase, whereas ALP is widely expressed in various types of cells.

As another labeling enzyme functioning in neutral pH, diaphorase (Dp) would be applicable in feedback-mode SECM. In this measurement mode, the probe electrode was set at +0.35 V to oxidize  $\text{FcCH}_2\text{OH}$  to  $[\text{FcCH}_2\text{OH}]^+$ , which was reduced again to  $\text{FcCH}_2\text{OH}$  by the Dp-catalyzed reaction at the cell membrane in the presence of NADH. This redox cycling generated additional oxidation current for  $\text{FcCH}_2\text{OH}$ . Figure 4 shows the SECM images of the patterned cell with Dp-labeled EGFR/CHO in the presence and absence of NADH. The addition of NADH

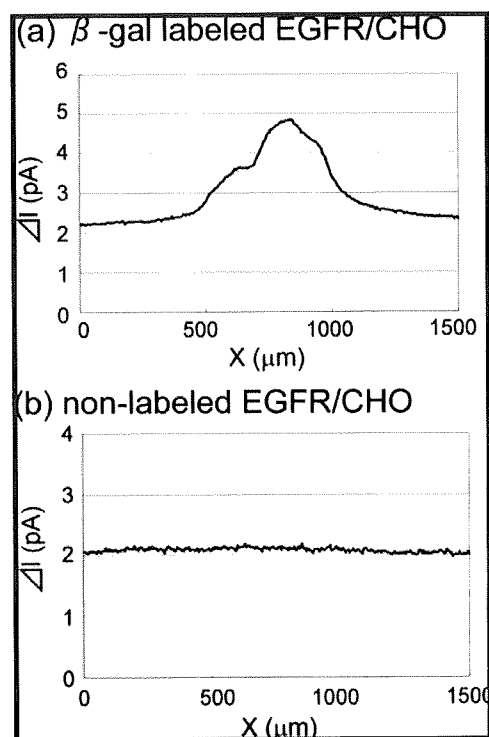


**Figure 3.** One-line scan of microstencil-patterned cells (a)  $\beta$ -gal-labeled EGFR/CHO and (b) nonlabeled EGFR/CHO in substrate generation/tip collection mode SECM. The electrode was set at 20  $\mu\text{m}$  above the substrate, and the scan rate was 10  $\mu\text{m/s}$ . The scan range was 1500  $\mu\text{m}$ .

significantly increased the current responses, indicating that Dp can also be used as a labeling enzyme for imaging EGFR/CHO cells. The small current response prior to adding NADH was probably caused by intracellular reduction of  $[\text{FcCH}_2\text{OH}]^+$  as it permeated through the cell membrane (see Supporting Information). In addition, we found that the current response for EGFR/CHO cells without enzyme labeling depends on the tip scan rate. This could be also because the  $\text{FcCH}_2\text{OH}$  penetrates the cell, and the tip electrode exhausts the redox inside the cell at a very slow scan rate. Similar problems occur when probing redox active thin-layer systems.<sup>40–43</sup>

**SECM Images of EGFR at the Cell Surface of a Single Living Cell.** Figure 5 shows single-cell imaging with the SECM substrate generation/tip collection mode for EGFR/CHO and normal CHO. ALP was selected as the labeling enzyme. The current response of the EGFR/CHO cell was considerably larger than that of normal CHO. This result indicated that SECM can distinguish the EGFR expression level of a single adhesion cell without peeling it from the dish. To our knowledge, there have been no other reports on the detection of specific proteins at the cell surface by using SECM-based ELISA, although SECM-based

(36) Liebetrau, J. M.; Miller, H. M.; Baur, J. E.; Takacs, S. A.; Anupunpisit, V.; Garris, P. A.; Wipf, D. O. *Anal. Chem.* 2003, 75, 563–571.

(37) Ciolkowski, E. L.; Cooper, B. R.; Jankowski, J. A.; Jorgenson, J. W.; Wightman, R. M. *J. Am. Chem. Soc.* 1992, 114, 2815–2821.

(38) Hengstenberg, A.; Blöchl, A.; Dietzel, I. D.; Schuhmann, W. *Angew. Chem., Int. Ed.* 2001, 40, 905–908.

(39) Kurulugama, R. T.; Wipf, D. O.; Takacs, S. A.; Pongmayteegul, S.; Garris, P. A.; Baur, J. E. *Anal. Chem.* 2005, 77, 1111–1117.

(40) Zhang, J.; Slevin, C. J.; Morton, C.; Scott, P.; Walton, D. J.; Unwin, P. R. *J. Phys. Chem. B* 2001, 105, 11120–11130.

(41) O'Mullane, A. P.; Macpherson, J. V.; Unwin, P. R.; Cervera-Mopntesinos, J.; Manzanares, J. A.; Frehill, F.; Vos, J. G. *J. Phys. Chem. B* 2004, 108, 7219–7227.

(42) Nijhuis, C. A.; Sinha, K. K.; Wittstock, G.; Huskens, J.; Ravoo, B. J.; Reinhoudt, D. N. *Langmuir* 2006, 22, 9770–9775.

(43) Zhang, M.; Wittstock, G.; Shao, Y.; Girault, H. H. *Anal. Chem.* 2007, 79, 4833–4839.

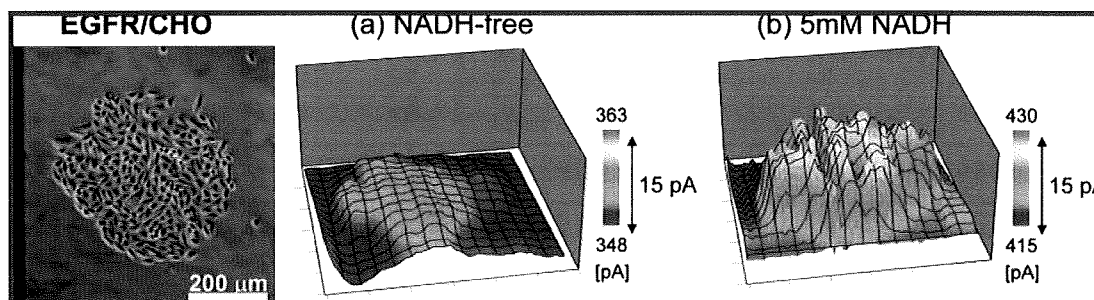


**Figure 4.** SECM feedback mode image of microstencil-patterned EGFR/CHO cells. EGFR/CHO cells imaged in the NADH-free solution and in 5 mM NADH solution. The electrode was set at 15  $\mu\text{m}$  above the substrate, and the scan rate was 50  $\mu\text{m}/\text{s}$ . The scan range was 600  $\mu\text{m}$   $\times$  600  $\mu\text{m}$ , and the step size was 10  $\mu\text{m}$ .

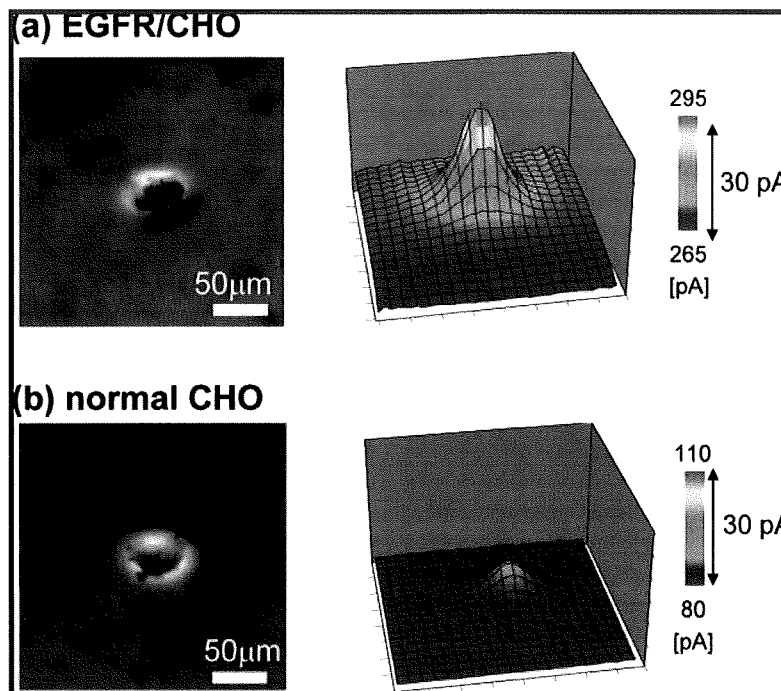


**Figure 5.** Single CHO cell SECM image in substrate generation/tip collection mode: (a) EGFR/CHO cell and (b) normal CHO cell. The electrode was set at 15  $\mu\text{m}$  above the substrate, and the scan rate was 5  $\mu\text{m}/\text{s}$ . The scan range was 200  $\mu\text{m}$   $\times$  200  $\mu\text{m}$ , and the step size was 5  $\mu\text{m}$ .

ELISA has been applied to detect antigens<sup>23–27</sup> and cytokines<sup>28</sup> on solid surfaces. The present study is the first to demonstrate SECM measurement of a cell membrane protein at the single-cell level.

Mammalian cells naturally show endogenous phosphatase activity that is significant in the context of SECM imaging at the single-cell level. Therefore, we corrected the EGFR expression signal by subtracting the current response of nonlabeled cells from that of ALP-labeled cells in a single-scan measurement. The peak currents of nonlabeled normal CHO, EGFR/CHO, and A431 cells were  $7.9 \pm 6.0$  pA ( $n = 5$ ),  $5.4 \pm 2.5$  pA ( $n = 3$ ), and  $6.8 \pm 0.8$  pA ( $n = 8$ ), respectively. These responses were considered background signals and subtracted from the current responses for ALP-labeled cells. Figure 6 shows the peak currents for ALP-labeled cells after subtraction. Significant differences were found in the responses for the three types of cells as follows: CHO < EGFR/CHO < A431 ( $p < 0.001$ , normal CHO and EGFR/CHO;  $p < 0.060$ , EGFR/CHO and A431). The same order of EGFR expression levels was also found in measurements by flow cytometry (see

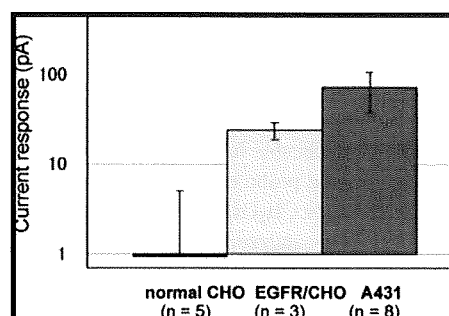


**Figure 6.** Relative EGFR expression level of a single cell measured by SECM in substrate generation/tip collection mode.

Supporting Information, Figure S1). The expression level for EGFR/CHO relative to that for A431 was 0.33, which was the same as that determined by flow cytometry. This agreement reinforces the conclusion that SECM measurement provides a reliable estimation of the EGFR expression levels. It should be noted that SECM provides quantitative, continuous information on single

living, single adherent cells without peeling them from the dish. In the future, the mapping of EGFR on the cell surface and the real-time monitoring of endocytosis induced by EGF stimulation will also be possible.

## CONCLUSION

In this study, we have described the membrane protein imaging of living cells with SECM. The expression level of EGFR at the cell surface of an adherent single cell was measured without peeling it from the culture dish by using enzyme-labeled antibodies. Furthermore, imaging at the single-cell level was successfully performed, demonstrating that the expression level is statically distinguishable in the following descending order: normal CHO, EGFR/CHO, and A431.

The formation of the EGF–EGFR complex triggers endocytosis and subsequent cell proliferation. Thus, real-time monitoring of EGFR density at the cell membrane affords quantitative information about the initial stage of cell signaling. Unlike fluorescence imaging, the SECM procedure described in the present study is, in principle, surface sensitive; therefore, it is advantageous in selectively detecting the processes occurring at the outer membrane surface. We think that SECM measurement is particularly suitable for monitoring EGF-triggered endocytosis, in which EGF induces entrapment of EGFR at the cell surface into the inside of the cell. Furthermore, because SECM is a versatile system that can be used not only for quantitative

membrane analysis but also for topographic or optical imaging<sup>44</sup> of cells and sample manipulation (including simultaneous injection/collection of biomolecules<sup>45</sup>), other membrane protein-related phenomena could also be continuously and successfully monitored by SECM.

## ACKNOWLEDGMENT

This work was partly supported by Grants-in-Aid for Scientific Research (Grants 18101006 and 19750055) from MEXT (Ministry of Education, Culture, Sports, Science and Technology), Japan; and by a grant from the Center for Interdisciplinary Research, Tohoku University. Y.T. acknowledges the support obtained from a research fellowship of the Japan Society for the Promotion of Science. The A431 cells and normal CHO cells were donated by the Institute of Development, Aging and Cancer, Tohoku University.

## SUPPORTING INFORMATION AVAILABLE

Additional information as noted in text. This material is available free of charge via the Internet at <http://pubs.acs.org>.

Received for review January 26, 2009. Accepted February 12, 2009.

AC900195M

(44) Takahashi, Y.; Hirano, Y.; Yasukawa, T.; Shiku, H.; Yamada, H.; Matsue, T. *Langmuir* 2006, 22, 10299–10306.

(45) Nashimoto, Y.; Takahashi, Y.; Yamakawa, T.; Torisawa, Y.; Yasukawa, T.; Tio-Sasaki, T.; Yokoo, M.; Abe, H.; Shiku, H.; Kambara, H.; Matsue, T. *Anal. Chem.* 2007, 79, 6823–6830.

# Transfected Single-Cell Imaging by Scanning Electrochemical Optical Microscopy with Shear Force Feedback Regulation

Yasufumi Takahashi,<sup>†</sup> Hitoshi Shiku,<sup>\*,†</sup> Tatsuya Murata,<sup>†</sup> Tomoyuki Yasukawa,<sup>†</sup> and Tomokazu Matsue<sup>\*,†</sup>

Graduate School of Environmental Studies, Tohoku University, Aramaki Aoba 6-6-11-605, Sendai 980-8579, Japan, and Graduate School of Material Science, University of Hyogo, 3-2-1 Kouto, Kamigori-cho, Ako-gun, Hyogo 678-1297, Japan

Gene-transfected single HeLa cells were characterized using a scanning electrochemical/optical microscope (SECM/OM) system with shear-force-based probe-sample distance regulation to simultaneously capture electrochemical, fluorescent, and topographic images. The outer and inner states of single living cells were obtained as electrochemical and fluorescent signals, respectively, by using an optical fiber-nanoelectrode probe. A focused ion beam (FIB) was used to mill the optical aperture and the ring electrode at the probe apex (the inner and outer radii of the ring electrode were 37 and 112 nm, respectively). To apply an appropriate shear force between the probe tip and the living cell surface, we optimized the amplitude of oscillation of the tuning fork to which the probe was attached. Field-programmable gate arrays (FPGA) were adopted to drastically increase the feedback speed of the tip-sample distance regulation, shorten the scanning time for imaging, and enhance the accuracy and quality of the living cell images. In employing these improvements, we simultaneously measured the cellular expression activity of both secreted alkaline phosphatase outside and GFP inside by using the SECM/OM with shear force distance regulation.

Scanning electrochemical microscopy (SECM) has been successfully used to investigate various biological systems because it allows the physiological conditions of localized chemical species to be quantitatively characterized in situ in a non-invasive manner.<sup>1–5</sup> Significant efforts have been made to improve the electrochemical measurement sensitivity, lateral resolution, and

quality of SECM by using nanoelectrodes<sup>6–11</sup> as scanning probes and by incorporating distance control mechanisms related to atomic force microscopy (AFM),<sup>12–15</sup> shear force,<sup>16–22</sup> faradaic current,<sup>23–25</sup> and impedance<sup>26–28</sup> to detect chemicals having very short life spans or those present in trace amounts, such as neurotransmitters,<sup>16,23</sup> NO,<sup>19</sup> and oxygen.<sup>17</sup> Ueda et al. observed the PC12 axons abnormally swollen topography using SECM/NSOM (near-field scanning optical microscopy)/AFM.<sup>14</sup> They proposed the possibility of characterizing living cells to obtain chemical information on the inner and outer states by means of electrochemical and optical measurements, receptivity studies, and

\* To whom correspondence should be addressed. Phone/Fax: +81-22-795-7209. E-mail: shiku@bioinfo.che.tohoku.ac.jp (H.S.); matsue@bioinfo.che.tohoku.ac.jp (T.M.).

<sup>†</sup> Tohoku University.

<sup>‡</sup> University of Hyogo.

- (1) Bard, A. J.; Mirkin, M. V. *Scanning Electrochemical Microscopy*, 1st ed.; Marcel Dekker, Inc.: New York, 2001.
- (2) Amemiya, S.; Bard, A. J.; Fan, F. R. F.; Mirkin, M. V.; Unwin, P. R. *Ann. Rev. Anal. Chem.* 2008, 1, 95–131.
- (3) Roberts, W. S.; Lonsdale, D. J.; Griffiths, J.; Higson, S. P. J. *Biosens. Bioelectron.* 2007, 23, 301–318.
- (4) Schulte, A.; Schuhmann, W. *Angew. Chem., Int. Ed.* 2007, 46, 8760–8777.
- (5) Wittstock, G.; Burchardt, M.; Pust, S. E.; Shen, Y.; Zhao, C. *Angew. Chem., Int. Ed.* 2007, 46, 1584–1617.

- (6) Shao, Y. H.; Mirkin, M. V.; Fish, G.; Kokotov, S.; Palanker, D.; Lewis, A. *Anal. Chem.* 1997, 69, 1627–1634.
- (7) Stevin, C. J.; Gray, N. J.; Macpherson, J. V.; Webb, M. A.; Unwin, P. R. *Electrochem. Commun.* 1999, 1, 282–288.
- (8) Katemann, B. B.; Schuhmann, T. *Electroanalysis* 2002, 14, 22–28.
- (9) Xiong, H.; Guo, J. D.; Kurihara, K.; Amemiya, S. *Electrochem. Commun.* 2004, 6, 615–620.
- (10) Wu, W. Z.; Huang, W. H.; Wang, W.; Wang, Z. L.; Cheng, J. K.; Xu, T.; Zhang, R. Y.; Chen, Y.; Liut, J. *Am. Chem. Soc.* 2005, 127, 8914–8915.
- (11) Ufheil, J.; Hess, C.; Borgwarth, K.; Heinze, J. *Phys. Chem. Chem. Phys.* 2005, 7, 3185–3190.
- (12) Macpherson, J. V.; Jones, C. E.; Barker, A. L.; Unwin, P. R. *Anal. Chem.* 2002, 74, 1841–1848.
- (13) Kueng, A.; Kranz, C.; Lugstein, A.; Bertagnolli, E.; Mizaikoff, B. *Angew. Chem., Int. Ed.* 2003, 42, 3237–3240.
- (14) Ueda, A.; Niwa, O.; Maruyama, K.; Shindo, Y.; Oka, K.; Suzuki, K. *Angew. Chem., Int. Ed.* 2007, 46, 8238–8241.
- (15) Zhao, X. C.; Petersen, N. O.; Ding, Z. F. *Can. J. Chem.* 2007, 85, 175–183.
- (16) Hengstenberg, A.; Blochl, A.; Dietzel, I. D.; Schuhmann, W. *Angew. Chem., Int. Ed.* 2001, 40, 905–908.
- (17) Takahashi, Y.; Hirano, Y.; Yasukawa, T.; Shiku, H.; Yamada, H.; Matsue, T. *Langmuir* 2006, 22, 10299–10306.
- (18) Lee, Y.; Ding, Z. F.; Bard, A. J. *Anal. Chem.* 2002, 74, 3634–3643.
- (19) Isik, S.; Schuhmann, W. *Angew. Chem., Int. Ed.* 2006, 45, 7451–7454.
- (20) Yamada, H.; Fukumoto, H.; Yokoyama, T.; Koike, T. *Anal. Chem.* 2005, 77, 1785–1790.
- (21) Oyamatsu, D.; Hirano, Y.; Kanaya, N.; Mase, Y.; Nishizawa, M.; Matsue, T. *Bioelectrochemistry* 2003, 60, 115–121.
- (22) Garay, M. F.; Ufheil, J.; Borgwarth, K.; Heinze, J. *Phys. Chem. Chem. Phys.* 2004, 6, 4028–4033.
- (23) Kurulugama, R. T.; Wipf, D. O.; Takacs, S. A.; Pongmayteegul, S.; Garris, P. A.; Baur, J. E. *Anal. Chem.* 2005, 77, 1111–1117.
- (24) Isik, S.; Etienne, M.; Oni, J.; Blochl, A.; Reiter, S.; Schuhmann, W. *Anal. Chem.* 2004, 76, 6389–6394.
- (25) Fan, F. R. F.; Bard, A. J. *Proc. Natl. Acad. Sci. U.S.A.* 1999, 96, 14222–14227.
- (26) Alpuche-Aviles, M. A.; Wipf, D. O. *Anal. Chem.* 2001, 73, 4873–4881.
- (27) Diakowski, P. M.; Ding, Z. F. *Phys. Chem. Chem. Phys.* 2007, 9, 5966–5974.
- (28) Osbourn, D. M.; Sanger, R. H.; Smith, P. J. S. *Anal. Chem.* 2005, 77, 6999–7004.

analysis of the relationship between intracellular  $\text{Ca}^{2+}$  concentration and neurotransmitter release. However, in their work, the electrochemical and fluorescent images of PC12 were captured in constant-height mode. The current profiles in the electrochemical image only reflected the topography of the neuron without providing any information on chemical characteristics.

Shear force distance regulation has enabled the successful imaging of living cellular surfaces with near-field scanning optical microscopy (NSOM),<sup>29–31</sup> but SECM imaging is still difficult because the apices of SECM electrodes are generally larger than NSOM fiber probes. We successfully imaged single-cell topography and respiration activity using a conical-shaped optical fiber electrode.<sup>17</sup> However, the sensitivity of conical-shaped electrodes is low because the ratio of the electrode surface area near the cellular surface is very small.<sup>32</sup> To circumvent this problem, the apex of the probe should be made of disk- or ring-shaped electrodes. In this study, we employed a focused ion beam (FIB) to mill the probe apex and form ring electrodes. FIB allows the milling of a specific region selectively under FIB observation.

For successful imaging of living cell topography with scanning force microscopy, the magnitude of force interaction between the probe and cell should, in general, be less than 30 nN.<sup>33</sup> Although several studies reported theoretical approaches to detect shear force using a tuning fork,<sup>34,35</sup> most of them involved the calculation of forces in an air state, which was apparently unsuitable for performing measurements of living cells. In this study, we optimized the operating conditions of the vibrating probe to detect shear forces against living cells when the probe approaches at different oscillation amplitudes.

The probe scanning program also plays an important role in the imaging of living cell topography. The standing approach (STA) mode, in which the probe repetitively approaches the sample surface and retracts at each point, is a promising method for imaging the convoluted surface topography of living cells.<sup>17,20</sup> Similar scanning methods were reported by other groups.<sup>18,36</sup> However, such image acquisition takes too much time as compared to conventional lateral scanning methods. To resolve this problem, Korchev et al. changed the step size during measurement by prescanning the scan area.<sup>37</sup> In our system, we improved the feedback regulation speed by incorporating field-programmable gate arrays (FPGAs).

In this study, the inner and outer functions of single living cells were evaluated using an optical fiber-nanoelectrode probe with a

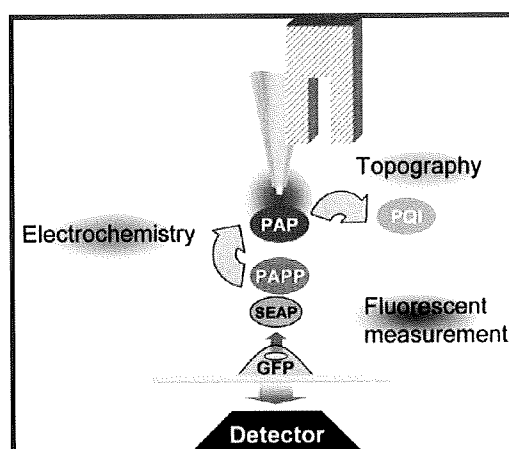


**Figure 1.** Schematic representation of simultaneous topographic, electrochemical, and optical imaging of a single transfected cell. Secreted alkaline phosphatase (SEAP) and green fluorescent protein (GFP) were cotransfected in HeLa cells.

shear force feedback system (Figure 1). This probe enables us to detect and induce electrochemical and photochemical reactions simultaneously. Smyrl et al. reported a photochemical study that used an SECM/optical microscope (OM) to realize a laser-induced photochemical reaction using an optical fiber and detect the reaction using a ring electrode.<sup>38,39</sup> In the present report, HeLa cells, transfected with two expression vectors including secreted alkaline phosphatase (SEAP) and green fluorescent protein (GFP), were used to demonstrate simultaneous topographic, electrochemical, and fluorescent imaging of living cells. SEAP has a unique feature that is secreted from the cell. Extracellular SEAP can be electrochemically detected by using *p*-aminophenylphosphate (PAPP) as a substrate.

## EXPERIMENTAL SECTION

**Chemicals.** *p*-Aminophenylphosphate monosodium salt (PAPP; LKT Laboratory Inc.) and ferrocenemethanol (FcMetOH; Aldrich) were purchased and used as received (as were all the other chemicals used in this study). All the solutions were prepared using distilled water obtained from a Milli-Q ultrapure water purification system (Millipore, Japan).

**Cell Culture and Transfection.** HeLa cells obtained from a human cervix epithelial cell line were cultured in Petri dishes (Falcon) with RPMI1640 medium (Gibco) containing 10% fetal bovine serum (FBS; Gibco), 50  $\mu\text{g mL}^{-1}$  penicillin, and 50  $\mu\text{g mL}^{-1}$  streptomycin in a humidified incubator (37 °C in an atmosphere of 5%  $\text{CO}_2$ ). The cells were trypsinized in a 0.25% trypsin solution and seeded ( $3 \times 10^5$  cells  $\text{mL}^{-1}$ ) onto culture plates such as protein-patterned substrates. HeLa cells were transfected with a GFP vector (pAcGFP1-N1, 4.7 kb, BD Sciences) or cotransfected with the GFP vector and pSEAP2-control vector (5.1 kb, BD Sciences). The cells were seeded in a 35-mm dish (Falcon) at a density of  $5 \times 10^5$  cells in 2 mL of RPMI-1640 medium containing 10% FBS without antibiotics. After cultivation for 1 day, transfection was performed by the

(29) Koopman, M.; Cambi, A.; de Bakker, B. I.; Joosten, B.; Figdor, C. G.; van Hulst, N. F.; Garcia-Parajo, M. F. *FEBS Lett.* 2004, 573, 6–10.

(30) de Bakker, B. I.; de Lange, F.; Cambi, A.; Korterik, J. P.; van Dijk, E. M.; van Hulst, N. F.; Figdor, C. G.; Garcia-Parajo, M. F. *ChemPhysChem.* 2007, 8, 1473–1480.

(31) de Bakker, B. I.; Bodnar, A.; van Dijk, E. M.; Vamosi, G.; Damjanovich, S.; Waldmann, T. A.; van Hulst, N. F.; Jenci, A.; Garcia-Parajo, M. F. *J. Cell Sci.* 2008, 121, 627–633.

(32) Mirlkin, M. V.; Fan, F. R. F.; Bard, A. J. *J. Electroanal. Chem.* 1992, 328, 47–62.

(33) Henderson, E.; Haydon, P. G.; Sakaguchi, D. S. *Science* 1992, 257, 1944–1946.

(34) Karrai, K.; Grober, R. D. *Appl. Phys. Lett.* 1995, 66, 1842–1844.

(35) Karrai, K.; Grober, R. D. *Ultramicroscopy* 1995, 61, 197–205.

(36) Borgwarth, K.; Ebling, D. G.; Heinze, J. *J. Ber. Bunsen-Ges. Phys. Chem.* 1994, 98, 1317–1321.

(37) Novak, P.; Li, C.; Shevchuk, A. I.; Stepanyan, R.; Caldwell, M.; Hughes, S.; Smart, T. G.; Gorelik, J.; Ostanin, V. P.; Lab, M. J.; Moss, G. W.; Frolenkov, G. I.; Klenerman, D.; Korchev, Y. E. *Nat. Methods* 2009, 6, 279–281.

(38) James, P. I.; Garfias-Mesias, L. F.; Moyer, P. J.; Smyrl, W. H. *J. Electrochem. Soc.* 1998, 145, L64–L66.

(39) James, P.; Casillas, N.; Smyrl, W. H. *J. Electrochem. Soc.* 1996, 143, 3853–3865.

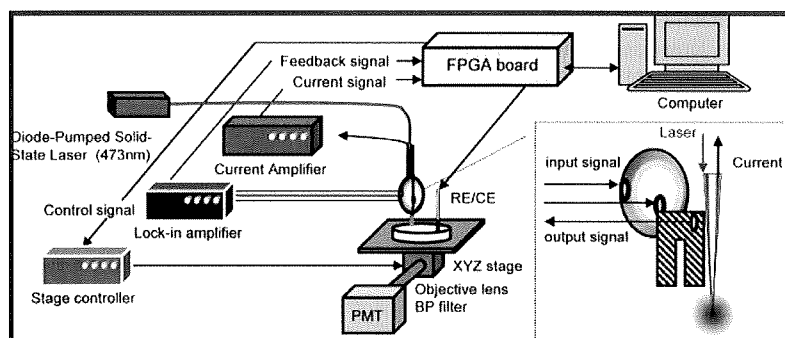


**Figure 2.** Schematic diagram of the SECM/OM system with shear force feedback regulation.

addition of 500  $\mu\text{L}$  of Opti-MEM I medium (Gibco) containing 4  $\mu\text{g}$  of plasmid DNA and 10  $\mu\text{L}$  of Lipofect AMINE 2000 (Invitrogen). The cells were then incubated at 37  $^{\circ}\text{C}$  overnight.

**Measurement System.** The configuration of the SECM/OM system with feedback control of probe-sample distance was basically the same as that reported previously.<sup>17</sup> A FPGA board (NI-7831R, National Instruments) was incorporated into the basic system to improve the speed of feedback regulation. A schematic diagram is shown in Figure 2. FPGA is a device that contains a matrix of reconfigurable gate array logic circuitry. It is capable of executing complex discrete signal processing algorithms with clock rates of 40 MHz at maximum. Probe-sample distance feedback control and data acquisition were achieved without compromising the performance of the main PC operation.

For topography measurement, the probe was attached to one of the prongs of a tuning fork and vibrated using a piezoelectric buzzer (0.5–1 mV p-p, sine wave) to drive the tuning fork into the resonance state. The resonance frequency of the unprocessed tuning fork was 32 768 (2<sup>15</sup>) Hz. The vibration signal from tuning fork was detected by a lock-in amplifier. The output time constant of the lock-in amplifier was set 3 ms. To synchronize the lock-in amplifier output signal with FPGA, the 3 ms signal from lock in amplifier was summed and leveled on FPGA.

**Probe Scanning Program.** We used the STA mode, which involves repetitive steps of approach toward the surface and retraction of the tip at each measurement point.<sup>20,40</sup> First, the probe position was set far from the sample, and the original tuning fork amplitude at a resonance frequency was measured (3 ms). The probe approached the sample until the tuning fork signal amplitude reduced to 1% of the original signal. The signal reduction is caused by the shear force between the probe tip and the sample surface. The approach process takes about 50–100 ms. The speed and accuracy of this process was enhanced dramatically by adopting the FPGA board. Next, the probe was lifted by 50 nm to acquire the current/optical signal for 100 ms. Vertical movement of the probe may be caused by liquid convection. Therefore, we waited 10 ms before recording the current/optical signal. The probe was further raised by about 0.1–3.0  $\mu\text{m}$  to avoid contacting the sample surface. By repeating these processes at every measurement point, the probe can follow the changing shape of the sample and maintain a constant distance to sample as noncontact.

(40) Takahashi, Y.; Miyamoto, T.; Shiku, H.; Asano, R.; Yasukawa, T.; Kumagai, I.; Matsue, T. *Anal. Chem.* 2009, 81, 2785–2790.

**Fabrication of an Optical Fiber Electrode.** A single-mode optical fiber (New Port, F-SA) was pulled using a carbon dioxide laser puller (Sutter Instruments, Model P-2000). The fiber was then coated with a Ti/Pt layer by sputtering (Anelva, L-332S-FH, RF200) and subsequently insulated with a xylene polymer (parylene C, Daisan Kasei) via vapor deposition polymerization (PDS-2010, Parylene Japan). To expose an electroactive area and form an optical aperture, the probe apex was milled by a focused ion beam (FIB, Seiko Instruments, SMI 2050).

**Measurement Methods of SEAP and GFP.** SEAP catalyzes the hydrolysis of PAPP to produce *p*-aminophenol (PAP), which is oxidized at a tip electrode potential of 0.3 V vs Ag/AgCl. The electrochemical detection of PAP allows the continuous quantification of SEAP expression in the genetically engineered cell. Concurrent with the electrochemical measurements, a laser light (wavelength = 473 nm) was introduced to excite GFP expressing inside the cell. Light emitted from the sample was collected by a photomultiplier tube (PMT, Hamamatsu H5920-01) through a long-pass filter (>520 nm) to obtain a fluorescent image.

## RESULTS AND DISCUSSIONS

To realize electrochemical and fluorescent detection of gene expression at the single-cell level, we tried to improve the sensitivity of the SECM/OM. First, we fabricated an optical fiber-nanoelectrode probe, which could simultaneously detect chemical information from the cellular surface and optical information from inside the cell. Second, the amplitude of tuning fork oscillation was optimized for shear-force-based distance regulation to trace the surface of the living cell. Third, improvement concerning the feedback speed for distance regulation by incorporating an FPGA board.

**Characterization of Optical Fiber Electrode.** Figure 3a shows a scanning electron microscopy (SEM) image of the optical fiber-nanoelectrode probe. The radii of the inner and outer rings of the electrode and the insulator layer were 37, 112, and 320 nm, respectively. Figure 3b shows the cyclic voltammogram (CV) of this electrode in 0.5 mM FcMeOH and 0.1 M KCl at a scanning rate of 20 mV/s. The steady state current (150 pA) was larger than that calculated for a 112 nm-radius disk electrode (16 pA). As the ratio of the outer-to-inner ring radius was much larger than 1.25, the edge effect peculiar to the ring electrode could not be seen; thus, the CV behavior of the ring electrode was almost the same as that of the disk electrode.<sup>41</sup> Figure 3c shows the tip current profile as a function of the tip-sample distance when the

(41) Lee, Y.; Amemiya, S.; Bard, A. J. *Anal. Chem.* 2001, 73, 2261–2267.

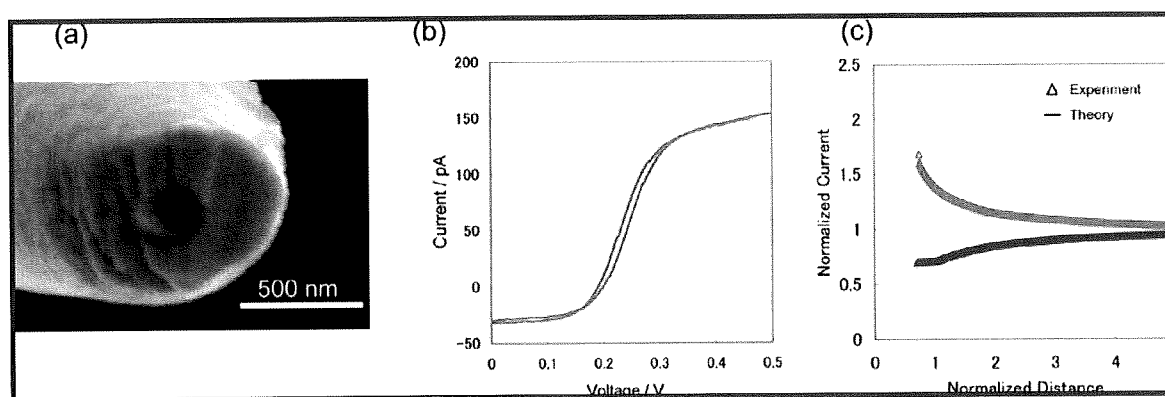


**Figure 3.** Characteristics of an optical fiber electrode. (a) Scanning electron microscopy micrograph. (b) Cyclic voltammogram of an optical fiber electrode probe in 0.5 mM ferrocenemethanol(FcMetOH) and 0.1 M KCl at a scan rate of 20 mV/s. (c) Approach curve of normalized current for Pt and glass substrates was plotted at a probe potential of +0.50 V (vs Ag/AgCl) in 0.5 mM FcMetOH and 0.1 M KCl. The tip-sample distance was normalized to the tip radius of 785 nm.

tip approaches the glass substrate. In this experiment, we used a 785 nm-radius electrode. This electrode steady state current (240 pA) was also larger than the theoretical one (112 pA). There is a possibility that the defects in the insulating layer at the side of the electrode caused larger current, although the defect of insulating layer was not able to observe using SEM. The smaller electrode (112 nm-radius, Figure 3b) tended to present a larger deviation in currents between the theoretically estimated from SEM image and the experimentally observed with amperometry than the larger electrode (785 nm-radius, Figure 3c).

In spite of a disagreement of the steady state current, both conductive and nonconductive samples demonstrated clearly visible feedback effects in their respective approach curves. The experimental curves were well fitted with the theoretical curves plotted with the assumption of RG 2.0 (RG, dimensionless insulator radius of the tip normal to the electrode radius of the tip).<sup>42</sup> Although several groups have reported the fabrication of nano-electrodes, few researchers have obtained approach curves that provide current changes because of positive or negative feedback at a tip-sample distance smaller than the tip radius. For probe electrodes of conical or hemispherical shape, feedback effects are not clearly visible. We tried to flatten the probe apex by milling with FIB to improve current sensitivity and spatial resolution. The FIB process increased the success rate of fabrication of the optical fiber-ring nanoelectrode probe by >90%. This electrode is suitable to detect cellular chemical properties.

**Optimization of the Shear Force during Tip-Sample Distance Regulation.** In shear force distance regulation, the amplitude of the tuning fork to which the probe is attached is the most important parameter for living cellular topography imaging. Damage to the cell increases when the tuning fork amplitude becomes larger. Therefore, the amplitude must be small enough to minimize the damage to the fragile cellular surface. However, when the amplitude was set at a very small value, the force caused by the solution viscosity interfered with the shear force detection. We investigated the correlation between the amplitude and the sensitivity of the tuning fork by using a glass capillary probe. As a sample, HeLa cells cultured in a 35-mm Petri dish filled with 2

mL RPMI medium were used. Figure 4a shows the approach curves obtained when the probe approaches the living cell surface at tuning fork amplitudes of 1 mV, 100  $\mu$ V, or 10  $\mu$ V. The tuning fork amplitude was normalized to the tuning fork amplitude of free oscillation in solution. When the probe approached the cell, the tuning fork amplitude reduced at the cell membrane surface ( $z = 8 \mu\text{m}$ ) and also significantly decreased at the bottom of the culture dish ( $z = 1 \mu\text{m}$ ). Importantly, when the tuning fork amplitude was set at 1 mV, the probe could not sense the cellular surface because the oscillation force was too strong to perform cell-surface measurements. When the tuning fork amplitude was set at 10  $\mu$ V, the force of solution viscosity interfered with the shear force detection and increased the noise level. Figure 4b shows topographies of HeLa living cells when the starting signal amplitudes of the tuning fork were adjusted to 30  $\mu$ V and 75  $\mu$ V. In shear-force-based distance regulation, the probe approached the surface until the tuning fork amplitude reduced to 1% of the original tuning fork amplitude. A clear image could be acquired when the tuning fork amplitude was set at 75  $\mu$ V. Random noises were evident in the image obtained at the amplitude of 30  $\mu$ V. When the tuning fork amplitude was set at 150  $\mu$ V, the topography could not be imaged (not shown). Therefore, the starting tuning fork amplitude was adjusted to about 70–80  $\mu$ V for imaging living cells. The optimal tuning fork amplitude depends on the design of the distance regulation probe, the shape of the probe, and the depth of the probe in the solution. Therefore, we carried out all experiments under the same conditions.

**Improvement of Feedback Speed during Distance Regulation.** Figure 5 shows the topography images of living HeLa cells observed using the shear force distance regulation system. Because of rapid FPGA data processing, the time required for imaging was drastically reduced when compared with the imaging time in the previous system without FPGA processing. Figure 5a shows the topography image of living mammalian cells in the range of  $100 \times 100 \mu\text{m}^2$  with 1- $\mu\text{m}$  stepsize (or 10 000 data points). The acquisition of shear-force signals to image the topography was completed within 30 min; thus, a 12-fold decrease in acquisition time was achieved as compared to the previous system. Moreover, higher resolution imaging can be

(42) Shao, Y. H.; Mirkin, M. V. *J. Phys. Chem. B* 1998, 102, 9915–9921.



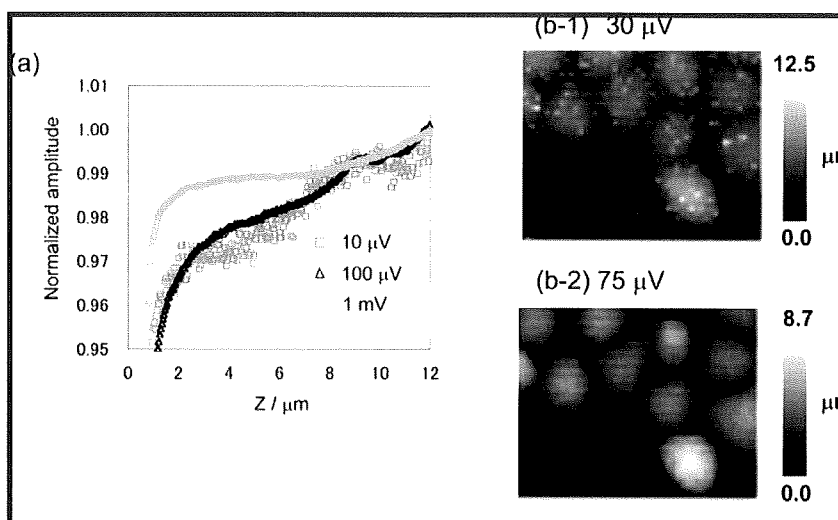


**Figure 4.** Optimization of tuning-fork amplitude for living cell topography imaging. (a) Tuning for amplitude-distance profiles of a living cellular surface. (b) Topography images of HeLa cells at tuning fork amplitudes of 30  $\mu\text{V}$  and 75  $\mu\text{V}$ . The scan range was 100  $\mu\text{m} \times 80 \mu\text{m}$ , and the step size was 2.0  $\mu\text{m}$ .

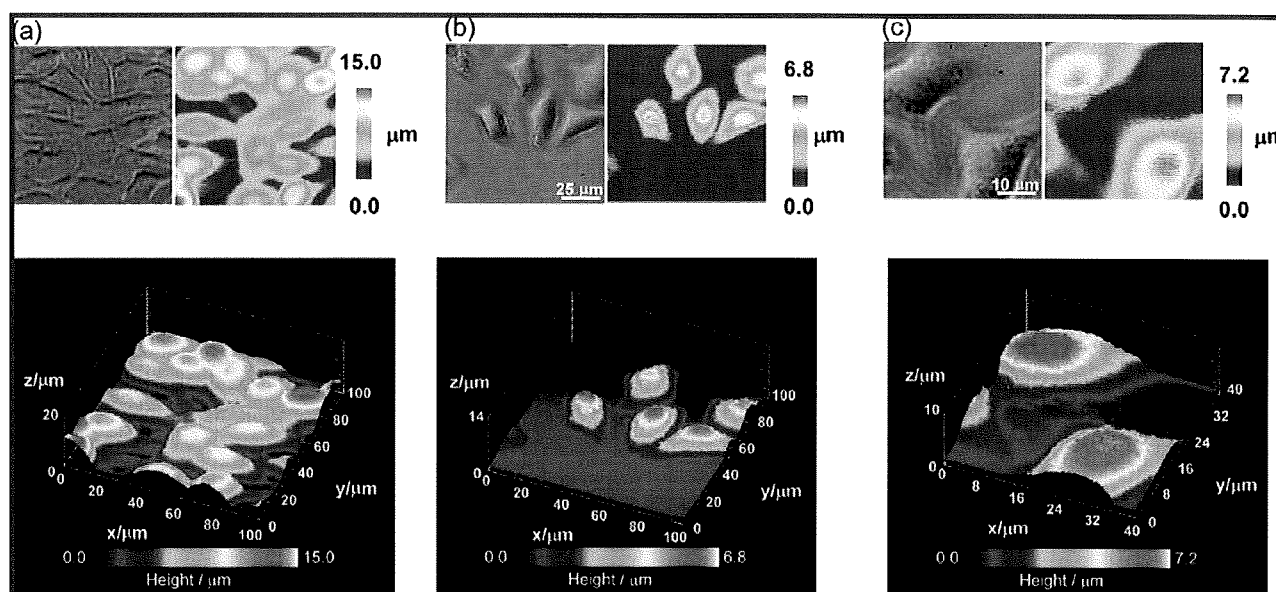


**Figure 5.** Optical micrograph and two- and three-dimensional topographically rendered images of (a) MCF-7 cells and (b, c) HeLa cells in a culture medium RPMI-1640 in the standing approach (STA) mode using a capillary probe. The respective scan ranges and step sizes were (a) 100  $\mu\text{m} \times 100$  and 1.0  $\mu\text{m}$ , (b) 100  $\mu\text{m} \times 100$  and 0.5  $\mu\text{m}$ , and (c) 40  $\mu\text{m} \times 40$  and 0.2  $\mu\text{m}$ .

realized because of the shorter imaging time. Figure 5b and c shows topography images with 0.5 and 0.2  $\mu\text{m}$  stepsize, respectively. The clear cellular surface topography images indicated that the maximum cellular height was approximately 7  $\mu\text{m}$ .

**GFP-Expressed HeLa Cell Images.** The expression of GFP in HeLa cells was measured in RPMI-1640 medium in constant-distance and constant-height modes. In the constant-height mode, the probe was positioned 10  $\mu\text{m}$  above the sample surface to prevent the probe tip from making contact with the sample surface during the scanning process. Figure 6 shows topographic and fluorescent images of HeLa cells. The cell topography conforms extremely well to the OM images of the cell. On the basis of the topography, the height of the HeLa cells was estimated to be 6.5  $\mu\text{m}$ . It should also be noted that the fluorescent images obtained

in the constant-distance mode (Figure 6c-1) were much sharper than those obtained in the constant-height mode (Figure 6c-2). The superiority of constant-distance imaging over constant-height imaging is evident in the cross-sectional fluorescence signals (Figure 7) at the lines indicated in Figure 6c. The half widths of the fluorescent peaks are found to be 18  $\mu\text{m}$  for the constant-distance mode and 31  $\mu\text{m}$  for the constant-height mode, indicating that distance regulation plays a crucial role in bioimaging based on fluorescence emission.

Since gene-expression levels in individual cells are influenced by intracellular processes such as transcription, translation, and postmodification, long-term monitoring of gene expression at the single-cell level is indispensable from the viewpoint of understanding intracellular signaling in greater detail. However, fluorescent

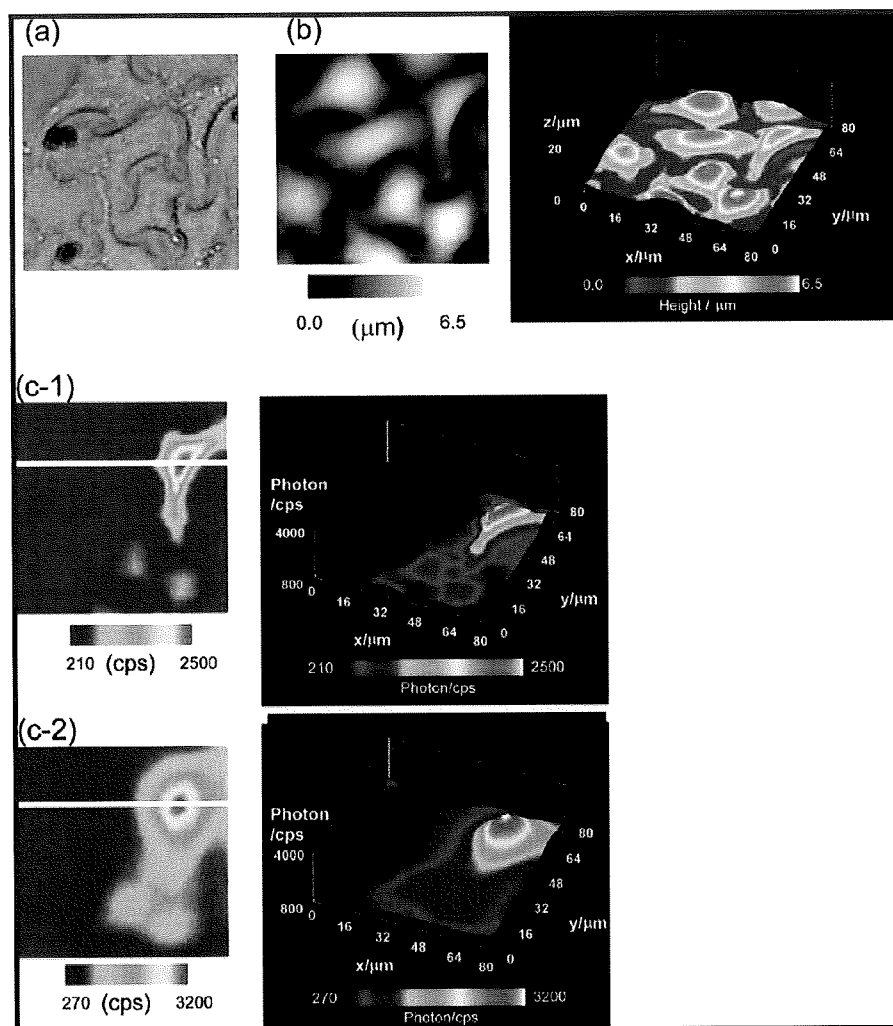


**Figure 6.** Optical (a), topographical (b), and two- and three-dimensional fluorescent (c) images of GFP-transfected HeLa cells. The topography image (b) was obtained by using shear force feedback distance modulation. Fluorescent images were obtained in the constant-distance mode (c-1) and constant-height mode (c-2). In the constant-height mode, the height was set at 10  $\mu\text{m}$  above the substrate, and the scan rate was 3  $\mu\text{m}/\text{s}$ . The scan range was 80  $\mu\text{m} \times 80 \mu\text{m}$ , and the step size was 1.0  $\mu\text{m}$ .

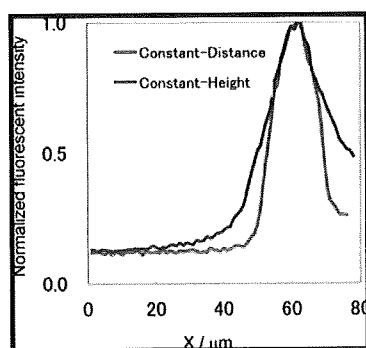


**Figure 7.** Cross-section of fluorescent signals of the image shown in Figure 6 in the constant-height and constant-distance modes. The fluorescent intensity was normalized with the maximum fluorescent intensity.

detection using a reporter protein such as GFP has serious drawbacks. First, it is unstable for long-term monitoring because excited light damages to the cell. Second, quantitative analysis is problematic because of photobleaching. Electrochemical detection

of gene expression, on the other hand, can be improved by using microarray-based systems with long-term monitoring, fast detection, and high throughput.<sup>43,44</sup> Furthermore, an electrochemical reporter system can be combined with other optical instruments used in the cotransfection reporter assay to provide a novel assay protocol, making it easy for us to distinguish specific reporter proteins.

**Simultaneous Detection of GFP and SEAP Coexpressed in a Single HeLa Cell.** Lipofection realizes cotransfection with two different vectors and has widely been used for investigating transcription factors, adhesion molecules, transporters, and protein-protein interactions.<sup>45,46</sup> Generally, cotransfection requires different reporter proteins in order to prevent gene

- (43) Torisawa, Y. S.; Ohara, N.; Nagamine, K.; Kasai, S.; Yasukawa, T.; Shiku, H.; Matsue, T. *Anal. Chem.* 2006, 78, 7625–7631.  
 (44) Lin, Z. Y.; Takahashi, Y.; Murata, T.; Takeda, M.; Ino, K.; Shiku, H.; Matsue, T. *Angew. Chem., Int. Ed.* 2009, 48, 2044–2046.  
 (45) Desai, M. A.; Burnett, J. P.; Mayne, N. G.; Schoepf, D. D. *Mol. Pharmacol.* 1995, 48, 648–657.  
 (46) Jones, F. S.; Prediger, E. A.; Bittner, D. A.; Derobertis, E. M.; Edelman, G. M. *Proc. Natl. Acad. Sci. U.S.A.* 1992, 89, 2086–2090.

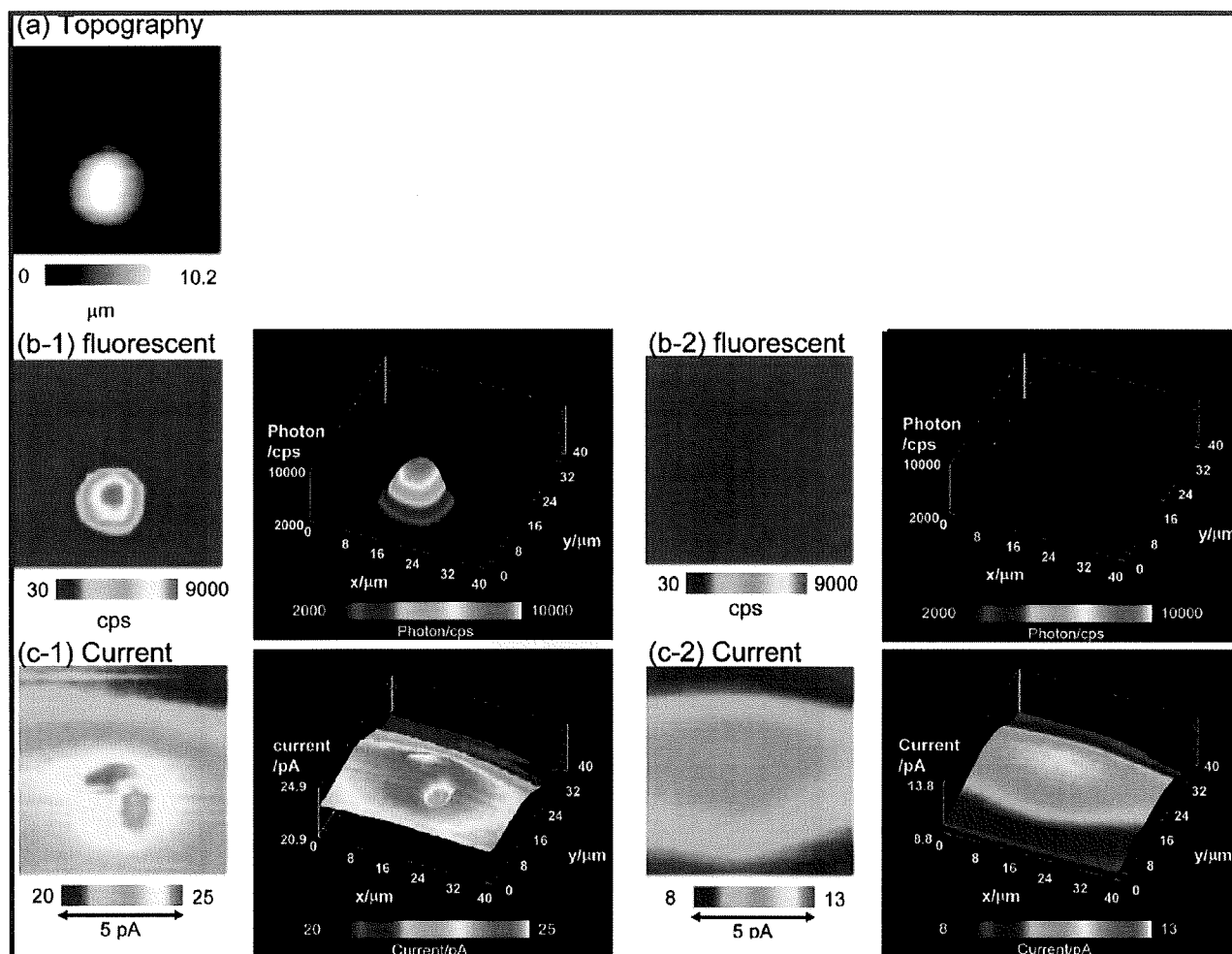


**Figure 8.** Simultaneous topographic (a), fluorescent (b-1 and b-2), and electrochemical (c-1 and c-2) images of a GFP- and SEAP-transfected single HeLa cell obtained in the constant-distance mode (a, b-1, and c-1) and constant-height mode (b-2 and c-2). In constant-height mode imaging, the height was set at  $15\ \mu\text{m}$  above the substrate, and the scan rate was  $3\ \mu\text{m/s}$ . The scan range was  $40\ \mu\text{m} \times 40\ \mu\text{m}$ , and the step size was  $1.0\ \mu\text{m}$ . The approximate inner and outer radii of the ring electrode were 200 and 480 nm, respectively.

expression from each vector. Although a set of fluorescence proteins with different colors has been employed to distinguish specific expressed proteins, there is a potential need to develop other detection methods for reporter proteins that are fundamentally different from fluorescent detection. Among other possible methods, electrochemical detection is a promising candidate. However, few reports have demonstrated that gene expression is electrochemically detectable at the single-cell level.<sup>47</sup> To our knowledge, the current study is the first to measure the gene expression of single cells based on fluorescence and electrochemistry.

Simultaneous topography, fluorescent, and electrochemical images of transfected single HeLa cells were obtained in constant-distance and constant-height modes (Figure 8). In the constant-height mode, the probe was positioned  $15\ \mu\text{m}$  above the sample surface and scanned in a HEPES-based saline solution (pH 9.5) containing 4.7 mM PAPP. When the probe moves above the HeLa cell, the intensity of the electrochemical signal increases as a result of the oxidation of PAPP generated by an enzyme reaction of

(47) Chang, C. Y.; Takahashi, Y.; Murata, T.; Shiku, H.; Chang, H. C.; Matsuo, T. *Lab Chip* 2009, 9, 1185-1192.

SEAP. Two-dimensional acquisition of the electrochemical signals provides SECM images of cells with high enzyme-expression capabilities. The time required to image a  $40 \times 40\ \mu\text{m}^2$  area with  $1\text{-}\mu\text{m}$  stepsize was typically 40 min. The constant-distance mode permits a higher contrast than the constant-height mode because the concentration of SEAP was high near the cell. Distance regulation is also important to improve electrochemical measurement sensitivity. The current response was found to decrease due to probe damping in the constant-distance mode when the probe approached the cell. Although we optimized our system for optical fiber electrode measurement, it was difficult to realize shear force distance regulation in the constant-distance mode because of the problems related to the structure of the probe and the solution in which measurements were carried out. For effective detection of shear force, we milled the probe at an angle of  $60^\circ$  to reduce the area of shear force interaction between the probe and the cell. Milling the probe to an angle of  $90^\circ$  resulted in interaction over a large area, due to which a clear signal corresponding to the shear force could not be obtained from the living cellular surface. In the present study, we used a HEPES-based saline solution with

pH 9.5, an optimum pH for SEAP. At this pH, the cellular membrane became unstable, although the cells remained alive for at least 3 h in the measuring solution. The membrane instability also gave rise to shear force instability and made constant-distance mode measurements impossible. Nevertheless, our study is the first to report simultaneous topographical, fluorescent, and electrochemical imaging of living cells with discrimination of the outer and inner cellular states.

## CONCLUSION

In this study, we simultaneously measured two reporter proteins, SEAP secreted from the cell to an outside solution and GFP expressed inside the cell, by using an SECM/OM system. Furthermore, we combined the system with shear force distance regulation to simultaneously detect topography, improved electrochemical responses, and fluorescent signals at the single-cell level. Previously, we reported the imaging of membrane proteins of living cells by using SECM.<sup>40</sup> The combination of fluorescent and electrochemical measurements is particularly useful for analyzing the dynamics of cellular membrane proteins, because the electrochemical response changes dramatically when the

membrane proteins move inside the cell. Future work will focus on membrane protein endocytosis by further developing the SECM/OM.

## ACKNOWLEDGMENT

This work was partly supported by Grants-in-Aid for Scientific Research (18101006 and 21685008) from MEXT (Ministry of Education, Culture, Sports, Science, and Technology), Japan, by a Grant-in-Aid for Scientific Research on Priority Areas (17066002) "Life Surveyor" from MEXT, and by a grant from the Center for Interdisciplinary Research, Tohoku University. Y.T. also acknowledges the support obtained from a research fellowship of the Japan Society for the Promotion of Science.

## SUPPORTING INFORMATION AVAILABLE

Characterization of tuning fork, amplitude and phase images of GFP- and SEAP-transfected single and simultaneous topographic, fluorescent, and electrochemical images of a GFP- and basic-SEAP-transfected single HeLa cell. This material is available free of charge via the Internet at <http://pubs.acs.org>.

Received for review August 9, 2009. Accepted October 10, 2009.

AC901796R



## Electrochemical single-cell gene-expression assay combining dielectrophoretic manipulation with secreted alkaline phosphatase reporter system

Tatsuya Murata<sup>a</sup>, Tomoyuki Yasukawa<sup>b</sup>, Hitoshi Shiku<sup>a,\*</sup>, Tomokazu Matsue<sup>a,\*\*</sup>

<sup>a</sup> Graduate School of Environmental Studies, Tohoku University, Aramaki Aoba 6-6-11, Sendai 980-8579, Japan

<sup>b</sup> Graduate School of Material Science, University of Hyogo, 3-2-1 Kouto, Kamigori-cho, Ako-gun, Hyogo 678-1297, Japan

### ARTICLE INFO

#### Article history:

Received 9 July 2009

Received in revised form 20 August 2009

Accepted 1 September 2009

Available online 6 September 2009

#### Keywords:

Scanning electrochemical microscopy

Single-cell analysis

Reporter

Dielectrophoresis

### ABSTRACT

Scanning electrochemical microscopy (SECM) was used for the analysis of single-cell gene-expression signals on the basis of a reporter system. We microfabricated a single-cell array on an Indium tin oxide (ITO) electrode comprising  $4 \times 4$  SU-8 microwells with a diameter of  $30 \mu\text{m}$  and a depth of  $25 \mu\text{m}$ . HeLa cells transfected with plasmid vectors encoding the secreted alkaline phosphatase (SEAP) were seeded in the microwell at a concentration of 1 cell per well by positive-dielectrophoresis (pDEP). A pDEP pulse of 3.0 Vpp and 1 MHz was applied between the microwell array/ITO electrode and an ITO counter electrode located on the top of the flow-cell assembly of the microdevice. The electrochemical responses of the individual HeLa cells transfected with SEAP were significantly larger than those of the wild-type HeLa cells. The electrochemical response of the transfected single cells was statistically distinguishable from that of wild-type HeLa cells. The size of the wells and the material of the single-cell array were optimized in order to evaluate the tumor necrosis factor  $\alpha$  (TNF- $\alpha$ )-induced activation process of nuclear factor kappa B (NF $\kappa$ B) that was used as the model for on-chip monitoring of cellular signal transduction.

© 2009 Elsevier B.V. All rights reserved.

### 1. Introduction

The living cell is itself an integrated sensing system by which highly sophisticated functional operation and parallel signal transduction pathways are systematically processed. Receptor proteins on the cell membrane or in the cytoplasm interact with specific ligand molecules, and consequently, this ligand-receptor binding induces conformational changes in proteins or in the molecular assembly. Reporter assay is frequently used in gene-expression studies; it involves incorporation of a vector plasmid carrying a reporter gene into the cells or the fusion of a promoter with the reporter gene. In a whole-cell reporter system, an analyte binds to a regulatory protein inducing reporter gene expression. Consequently, the reporter protein generates a detectable signal that can be measured by techniques such as photometry, radiometry, fluorescence, or colorimetry (Daunert et al., 2000). We selected alkaline phosphatase, which catalyzes the hydrolysis of phosphoric group, as the reporter enzyme (Kelso et al., 2000; Torisawa et al., 2006; Neugebauer et al., 2009). Secreted alkaline phosphatase (SEAP) hydrolyzes *p*-aminophenylphosphate (PAPP) to *p*-aminophenol (PAP), which is an electrochemically active species.

On these lines, we attempted to construct an electrochemical detection system by using microelectrode scanning technique (Torisawa et al., 2006; Shiku et al., 2009) and an electrochemical device (Lin et al., 2008, 2009; Yasukawa et al., 2008). In the present study, single-cell imaging of HeLa cells transfected with SEAP was performed by scanning electrochemical microscopy (SECM) (Bard et al., 1989; Mauzeroll and Bard, 2004; Bard et al., 2006; Li and Bard, 2009; Wittstock et al., 2007; Roberts et al., 2007; Takahashi et al., 2006, 2009) and compared with the concurrent responses of the wild-type HeLa cells.

Miniaturized well array and microfluidics have been shown to improve the throughput, sensitivity, and cost performance of single-cell analysis (Sims and Allbritton, 2007). Various techniques have been applied for constructing single-cell arrays (Whitaker and Walt, 2007; Retting and Folch, 2005; Ino et al., 2008; Matsunaga et al., 2008; Hosokawa et al., 2009; Sasuga et al., 2008; Yamamura et al., 2005; Skelley et al., 2009; Kovac and Voldman, 2007; Di Carlo et al., 2006). In the present study, we used positive-dielectrophoresis (pDEP) (Matsue et al., 1993, 1997; Matsumoto et al., 1994; Lee et al., 2008, 2009; Kunikata et al., 2009) for single-cell manipulation. It is generally believed that single-cell manipulation by DEP preserves the viability of the cells and their normal functions (Suzuki et al., 2008; Gray et al., 2004; Kaff and Voldman, 2005). Using statistical analysis, we have successfully distinguished the electrochemical response of the transfected single cells from that of wild-type HeLa cells. Signal transduction was also examined using single-cell array, where tumor necrosis factor  $\alpha$  (TNF- $\alpha$ )-induced activation of the

\* Corresponding author. Fax: +81 22 795 6167.

\*\* Corresponding author.

E-mail addresses: [shiku@bioinfo.che.tohoku.ac.jp](mailto:shiku@bioinfo.che.tohoku.ac.jp) (H. Shiku), [matsue@bioinfo.che.tohoku.ac.jp](mailto:matsue@bioinfo.che.tohoku.ac.jp) (T. Matsue).

nuclear factor kappa B (NF $\kappa$ B) pathway was the model pathway for single-cell array analysis. The optimum material for the construction of the single-cell chamber array was determined. Our findings indicate that accurate analysis of signal transduction may be hindered by DEP manipulation and the SU-8 as material for the construction of the array, both of which may cause elevation in the background level of SEAP expression before TNF- $\alpha$  stimulation.

## 2. Experimental

### 2.1. Chemicals and materials

*p*-Aminophenol (PAP; Wako Pure Chemical Industries), 3,3,4,4,5,5,6,6,6-nonafluorohexyl trichlorosilane (LS-912; Shin-Etsu Chemical Co. Ltd.), 2-[4-(2-hydroxyethyl)-1-piperazinyl] ethanesulfonic acid (HEPES; Dojindo Laboratories, Japan), SU-8 (Microchem), SU-8 developer (Microchem), SU-8 sheet (XP film TRIAL-25; KAYAKU MICROCHEM Co. Ltd., Japan), poly(dimethylsiloxane) (PDMS; Silpot 184W/C, Dow Corning, USA), tumor necrosis factor- $\alpha$  (TNF- $\alpha$ ; Wako Pure Chemical Industries), RPMI-1640 (Gibco Invitrogen, Tokyo, Japan), fetal bovine serum (FBS; Gibco), penicillin/streptomycin (Gibco), phosphate buffered saline (PBS(-)); Wako Pure Chemical Industries), calcein-acetoxymethyl ester (calcein-AM; Dojindo Laboratories), propidium iodide (PI; Dojindo Laboratories), Opti-MEM 1 medium (Gibco), Lipofectamine™ 2000 (Invitrogen), and other chemicals were used as received. SEAP control vector (pSEAP2-Control) and the pNF $\kappa$ B-SEAP plasmid vector, in which a transfer element binding the  $\kappa$ B site of the NF $\kappa$ B was located upstream of the SEAP reporter gene, were purchased from Clontech, BD Sciences. Indium tin oxide (ITO) electrode (4.50–4.98  $\Omega$ /sq) was purchased from Sanyo Vacuum Industries Co., Ltd. *p*-Aminophenylphosphate monosodium salt (PAPP) was purchased from LKT Lab Inc. or donated by Prof. Uichi Akiba from Akita University.

### 2.2. Cell culture and transfection

HeLa cells were donated by the Cell Resource Center for Biomedical Research (Tohoku University). The cells were

cultured in RPMI-1640 containing 10% FBS and 50  $\mu$ g mL<sup>-1</sup> penicillin/streptomycin at 37 °C under a 5% CO<sub>2</sub> humidified atmosphere. The cultured HeLa cells were seeded in a 35-mm dish (Falcon) at a density of  $5 \times 10^5$  cells in 2 mL of antibiotic-free RPMI-1640 medium containing 10% FBS. On the subsequent day, the cells were transfected with 500  $\mu$ L of Opti-MEM 1 medium containing 4  $\mu$ g of plasmid DNA and 10  $\mu$ L of Lipofectamine™ 2000 and incubated for a further 5 h. Subsequently, the transfection medium was replaced by a fresh culture medium and the cells were incubated overnight at 37 °C.

### 2.3. Fabrication of single-cell array

We fabricated 3 types of array chips: microwell array/ITO, PDMS microwell array, and PDMS microstencil/polystyrene. The microwell array/ITO chip was designed to allow single-cell manipulation by pDEP. The microwell array/ITO chip with  $6 \times 4$  or  $6 \times 6$  arrays of cylindrical SU-8 microwell chambers was microfabricated on an ITO electrode. Each SU-8 microwell array (depth, 15 or 25  $\mu$ m; diameter, 20, 30, 50 or 100  $\mu$ m; gap between wells, 100  $\mu$ m) was photolithographically patterned onto the ITO electrode as follows: the ITO electrode was either spin-coated with SU-8 or pasted with a SU-8 sheet at 50 °C and subsequently prebaked on a hotplate at 95 °C for 5 min. Then, the SU-8 layer was exposed to UV light for 30 s using a mask aligner, and the SU-8 coating was removed by using an SU-8 developer. The SU-8 microwell array/ITO chip was assembled with a 30  $\mu$ m-thick poly(ethylene terephthalate) (PET) spacer and an ITO electrode on the top to construct a flow-through device (Fig. 1a). In order to pattern the cells with pDEP, the cells were suspended in a 0.2 M sucrose solution and injected into the device (Fig. 1a). pDEP manipulation was performed by applying an alternate current (AC) voltage (3 Vpp, 1 MHz) to the SU-8 microwell array/ITO chip and the top ITO electrode, in phase opposition so that the charge on each electrode is opposed at all times allowing the cells to deposit selectively in the microwells (Fig. 1b). After the wells were completely filled with cells, the current was turned off, and the cells outside the wells were removed by a slow-flowing stream of the medium (Fig. 1c). After disassembling the device, the

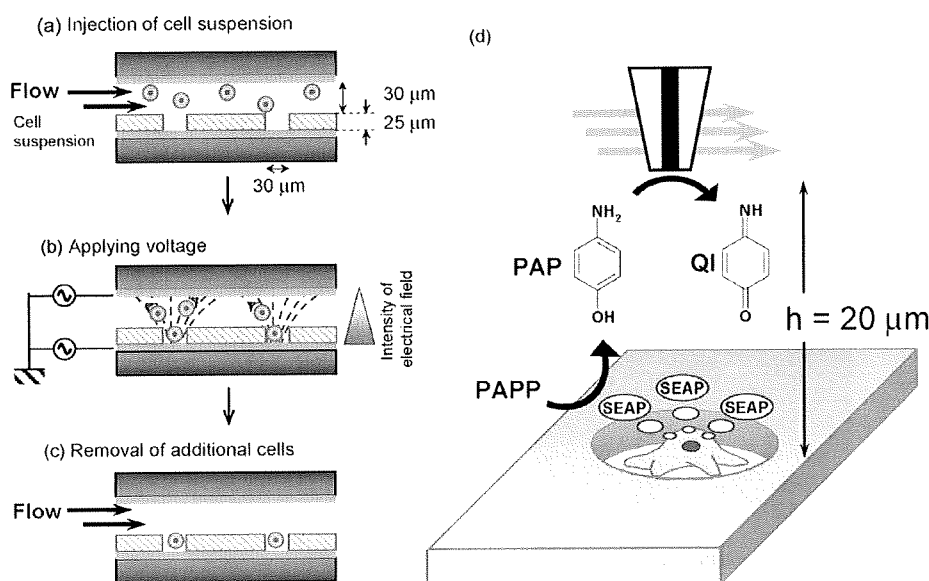


**Fig. 1.** Characterization of a reporter system using a single-cell array and electrochemical device. (a–c) Cell manipulation by pDEP; (d) the expression of the reporter enzyme SEAP is monitored electrochemically. PAPP was enzymatically hydrolyzed to produce PAP which was oxidized at +0.3 V vs. Ag/AgCl with the probe microelectrode. QI represents the product of electrooxidation. The height (*h*) of the electrode tip in the constant-height mode SECM was set at 20  $\mu$ m from the top of the SU-8 or PDMS microwells.

cells in the microwell were incubated with the medium at 37 °C under 5% CO<sub>2</sub> for 5–7 h.

The PDMS microwell array without the ITO electrode was prepared by the same method as mentioned above and fabricated by using a SU-8 master on a silicon wafer. The SU-8 master was first treated with a silane coupling agent (LS-912) to prevent PDMS from adhering to the master. Next, the PDMS prepolymer was poured on the SU-8 master and cured in the oven at 80 °C for 2 h. After curing, the PDMS replica was removed from the SU-8 master and treated with O<sub>2</sub> plasma in an asher. The resultant replica was used as the PDMS microwell array. The PDMS microstencil/polystyrene chip was fabricated by placing a PDMS stencil on a polystyrene culture dish (Falcon). The PDMS microstencil/polystyrene array was washed using ethanol and dried in the oven; finally, the surface of the PDMS stencil was treated with O<sub>2</sub> plasma in an asher.

The medium containing the cultured cells was poured over the PDMS microwell array or PDMS microstencil/polystyrene. After the cells were trapped in the microwells or the stencil, the surface was rinsed with a fresh medium to remove the additional cells, and the retained cells were cultured in the incubator at 37 °C under 5% CO<sub>2</sub> for 5–7 h. In the case of additional chemical stimulation to the cell, we continued the additional incubation of the cell array in the medium with chemicals (Shiku et al., 2009; Folch et al., 2000).

#### 2.4. SECM analysis of the single-cell reporter assay

The single cells in the microwell array were further studied by scanning electrochemical microscopy (Fig. 1d). The single cells captured in the individual microwells of the array were washed with HEPES buffer (150 mM NaCl, 4.2 mM KCl, 2.7 mM MgCl<sub>2</sub>,

1.0 mM Na<sub>2</sub>HPO<sub>4</sub>, 11.2 mM glucose, 10 mM HEPES, pH 7.0) and incubated in the same solution at 37 °C under 5% CO<sub>2</sub> atmosphere for 10 min. After incubation, the single-cell array was placed in 3 mL of a measuring solution containing 4.7 mM PAPP and HEPES buffer (pH 9.5). A two-electrode system comprising a Pt microdisk (diameter, 20 μm) as the working electrode and an Ag/AgCl reference/counter electrode was employed for the SECM measurements. The potential of the working electrode was set at 0.3 V vs. Ag/AgCl for facilitating the oxidation of PAP. An area of 600 μm × 450 μm or 600 μm × 600 μm was scanned by SCEM at a rate of 20 μm s<sup>-1</sup> at room temperature. The pixel unit of the image was 10 μm × 10 μm. The height of the electrode tip in the constant-height mode SECM was set at 20 μm from the top of the SU-8 or PDMS microwells.

#### 2.5. Live/dead fluorescence assay on single-cell arrays

The viability of the cells patterned on the stencil, under the conditions maintained during SECM measurements, was evaluated using a live/dead fluorescence kit (a combination of 2 fluorochromes, namely, calcein-AM and PI was used; Dojindo Laboratories, Japan). In the case of HeLa cells seeded in single-cell array with the PDMS microwell, almost all cells were alive (94%) for a period of 60 min after being soaked in the measuring solution (pH 9.5). It was also found that only 40% were alive for the single-cell array with the PDMS microwell, whereas more than 90% were alive for the cells patterned on a culture dish using a PDMS stencil of 300-μm diameter (Shiku et al., 2009), with the 120-min incubation in the measuring solution (pH 9.5) for 120 min at room temperature.

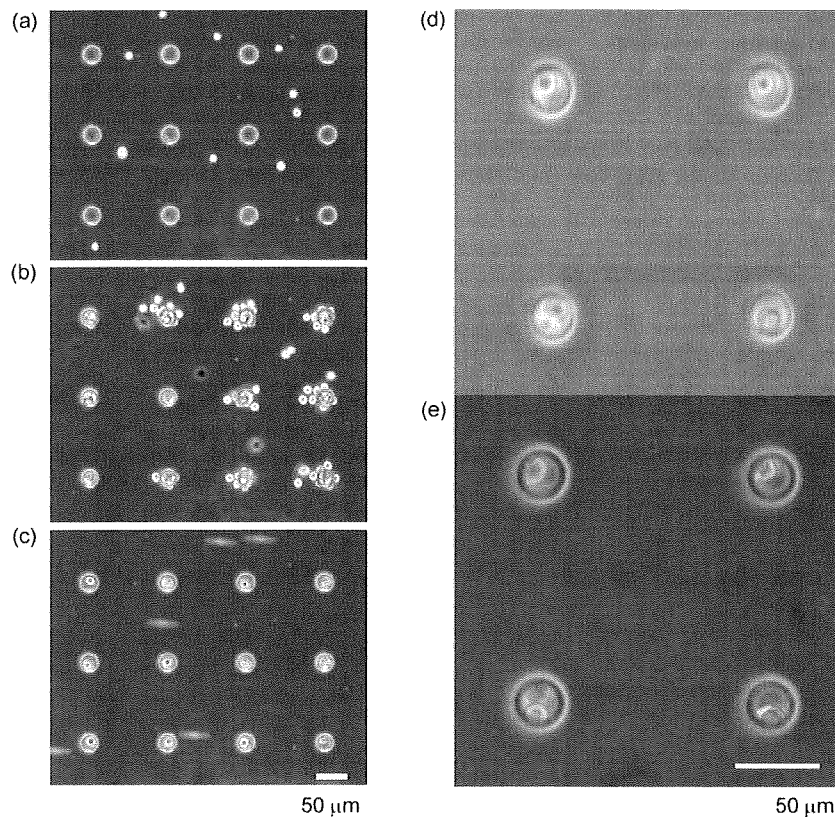


**Fig. 2.** (a–c) Sequential photographs acquired during the pDEP manipulation of cells on the SU-8 microwell array/ITO. (d) The single-cell array just after pDEP pulse application and the subsequent removal of the counter ITO electrode. (e) The cells after 5-h incubation in the culture medium. The diameter and depth of the microwells were 30 μm and 25 μm, respectively.

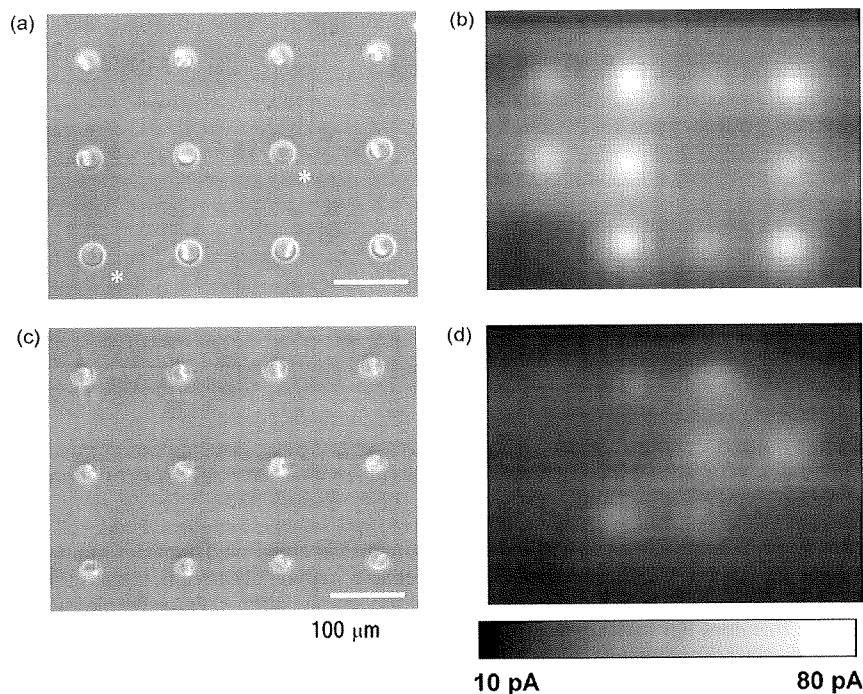


**Fig. 3.** Optical (a and c) and SECM images (b and d) of the single-cell array of HeLa-SEAP (a and b) and wild-type HeLa (c and d) cells on the SU-8 microwell array/ITO. SECM was performed in 4.7 mM PAPP, HEPES buffer (pH 9.5). The tip of the microelectrode (diameter, 20  $\mu\text{m}$ ) was used for scanning the cells from a 20  $\mu\text{m}$  height and at a scan rate of 20  $\mu\text{m s}^{-1}$ . The SECM scan area was 600  $\mu\text{m} \times 450 \mu\text{m}$ . The diameter and depth of the microwell were 30 and 25  $\mu\text{m}$ , respectively. The vacant well was marked as (\*).

### 3. Results and discussion

Fig. 2 shows the sequential photographs acquired during cell manipulation with pDEP. The cell suspension (density:  $5 \times 10^6$ – $5 \times 10^5$  cells  $\text{mL}^{-1}$  of 0.2 M sucrose) was introduced into the flow-through device comprising the microwell array/ITO and a top ITO electrode, and an AC voltage (3 Vpp, 1 MHz) was applied between the 2 electrodes (Fig. 2a). The phase shift between the AC voltages applied to the 2 electrodes was set at  $180^\circ$  by using a pulse generator (Hioki E.E.). The surface of the well array/ITO was treated with  $\text{O}_2$  plasma (Plasma asher, Yanaco). Within 10–20 s, the cells aggregated near the cylindrical microwell (Fig. 2b); subsequently, the AC voltage was turned off and the excess cells were removed by washing with a medium (Fig. 2c). The positive force generated during DEP was strong enough to retain the captured cell in the microwell even after the pulse was turned off. A simultaneous fluorescence viability assay indicated that the cells were alive and not damaged seriously as shown later. Fig. 2d shows a magnified view of the cells on the SU-8 microwell array/ITO just after pDEP manipulation; each microwell is observed to contain a single cell. Then, the top ITO electrode was removed and the single-cell array was soaked in culture medium and incubated for a further 5 h to promote active cellular adhesion to the electrode (Fig. 2e).

Next, the diameter and the height of the SU-8 wells were optimized. We constructed microwells with diameters of 20, 25, 30, 50, and 100  $\mu\text{m}$  and depths of 10 and 25  $\mu\text{m}$ . Fig. S-1 shows the arrays of cells formed by pDEP manipulation in the microwells with a depth of 25  $\mu\text{m}$  and different diameters. Only a single cell was captured in microwells with diameter of 20  $\mu\text{m}$  (Fig. S-1a) or 25  $\mu\text{m}$ , as the diameter of the HeLa cell was ca. 20  $\mu\text{m}$ . However, during washing, the entrapped cells were easily released from the wells. In addition, the cells tended to demonstrate apoptotic changes, since the well was too small for their survival (Chen et al., 1997; Nishizawa et al., 2002).

In microwells with a diameter of 30  $\mu\text{m}$ , a single cell was captured because there was no room to accommodate another cell. As already shown in Fig. 2, application of the DEP pulse attracted many cells to the microwell; the excess cells were easily flushed out by a slow-flowing stream of the sucrose solution. After 5-h incubation in the culture medium, the cells were observed to adhere to the substrate, and the formation of lamellipodium was noted on the electrode (Fig. S-1b). Further, good cellular attachment on the electrode was also observed in the case of wells with a diameter of 50  $\mu\text{m}$ , but an average of 3 cells were captured in these wells (Fig. S-1c). In the case of 100- $\mu\text{m}$  diameter wells, the DEP force was effective at the edge of the electrode (Fig. S-2), and hence the cell number in these wells showed a broad distribution. Fig. S-1d shows the relation between the occupancy rate and the cell number in microwells of various sizes. The occupancy rate was defined as the percentage of the microwell occupied with a certain number of the cell (0–6 cells) out of the all microwells observed. The rates for single-cell occupancy were high in the case of microwells with diameters of 20 or 30  $\mu\text{m}$ . Similar findings were noted for the microwells with a depth of 10  $\mu\text{m}$ . However, the cells in the 10- $\mu\text{m}$  deep microwells were easily flushed out by the washing or disassembling process (Chang et al., 2009). These results indicate that the single-cell array was most efficient when the microwells in the array chip had a diameter of 30  $\mu\text{m}$  and a depth of 25  $\mu\text{m}$ .

The viability of the cells in the microwell after pDEP was evaluated by using the live/dead fluorescence assay (Kaya et al., 2003; Torisawa et al., 2007). In order to determine the effects of the electric field and the dimensions of the microwell separately, we prepared 3 types of microwell arrays: microwell array/ITO, PDMS microwell array, and PDMS microstencil/polystyrene. We used the microwell array/ITO to evaluate the effect of the electric field; most of the entrapped single cells were alive (89.2%,  $n = 137$ ), and this result was in accordance with those of a previous study (Gray et al., 2004). In the case of the PDMS microwell array and the PDMS microstencil/polystyrene, 100% and 98% of the entrapped cells were



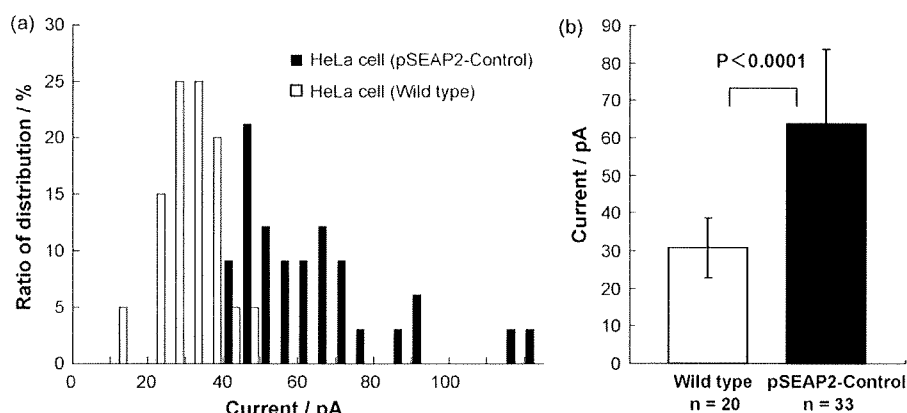


**Fig. 4.** (a) Histograms showing the ratio of distribution vs. the current response of HeLa-SEAP cells (filled bar) and wild-type HeLa cells (open bar) of the single-cell array on the SU-8 microwell array/ITO. (b) The average current response of HeLa-SEAP cells (filled bar,  $n = 33$ ) and wild-type HeLa cells (open bar,  $n = 30$ ). Error bar indicates the standard deviation.

alive, respectively. (See Supporting Information, Figs. S-3 and S-4.) The live/dead fluorescence assay revealed no significant difference between the viability of the cells among the 3 types of microwell arrays. However as shown later, this does not indicate that pDEP cellular manipulation is a stress-free technique against any cell line.

Next, we performed an electrochemical reporter assay on the single-cell array. HeLa cells (HeLa-SEAP) transfected with the plasmid vector (pSEAP2-control) containing the SEAP construct were selected for the reporter assay. The pSEAP2-control constitutively expressed the SEAP gene. The HeLa-SEAP and wild-type HeLa cells were independently localized on the  $4 \times 4$  single-cell array device by pDEP manipulation. The cells were cultivated in culture medium for 5 h at  $37^\circ\text{C}$ , and subsequently the device was soaked in 4.7 mM PAPP, HEPES buffer (pH 9.5). The cells remained alive for at least 1 h. A Pt electrode with 20- $\mu\text{m}$  diameter was used for scanning the cells in the SU-8 microwell from a height of 20  $\mu\text{m}$  at a scan rate of  $20 \mu\text{m s}^{-1}$ . The potential of the tip of the Pt electrode was set at +0.3 V vs. Ag/AgCl. Fig. 3 shows the optical and SECM images of the single-cell array of HeLa-SEAP and wild-type HeLa cells suspended in 4.7 mM PAPP, HEPES buffer (pH 9.5). The diameter and depth of the SU-8 microwell were 30  $\mu\text{m}$  and 25  $\mu\text{m}$ , respectively. The PAP oxidation current responses were well corresponding to the position of the microwell. Although the planar design of the cul-

ture dish enabled single-cell SECM imaging for detecting the SEAP reporter activity of the cells, it was difficult to control the cell density of these cultures. For example, since the cells were at stages immediately after cell division, they were located very close to each other, which made it impossible to resolve the current response of the 2 newly formed cells. Moreover, elevation of the background response was also a problem because PAP was continuously produced by the hydrolysis of PAPP via SEAP catalysis. Fig. 4 shows the distributions of the current responses of single HeLa-SEAP and wild-type HeLa cells. The ratio of distribution was defined as the percentage of the single-cell sample with a certain range of the current responses out of the all the SECM measurements. The average  $\pm$  standard deviation (SD) values for HeLa-SEAP and wild-type HeLa cells were  $63.64 \pm 20.06$  (filled bar,  $n = 33$ ) and  $30.77 \pm 7.88$  pA (open bar,  $n = 20$ ), respectively. The current response of the HeLa-SEAP cell was significantly larger than that of the non-transfected HeLa cell.

Single-cell SECM imaging and cell metabolism measurements have been already reported previously (Yasukawa et al., 1998; Kaya et al., 2003; Zhou et al., 2003; Bard et al., 2006; Schrock and Baur, 2007; Schulte and Schuhmann, 2007). Adherent cells show diverse distributions in the size, shape and cellular cycle phase. Therefore platform to arrange single-cell array becomes a useful

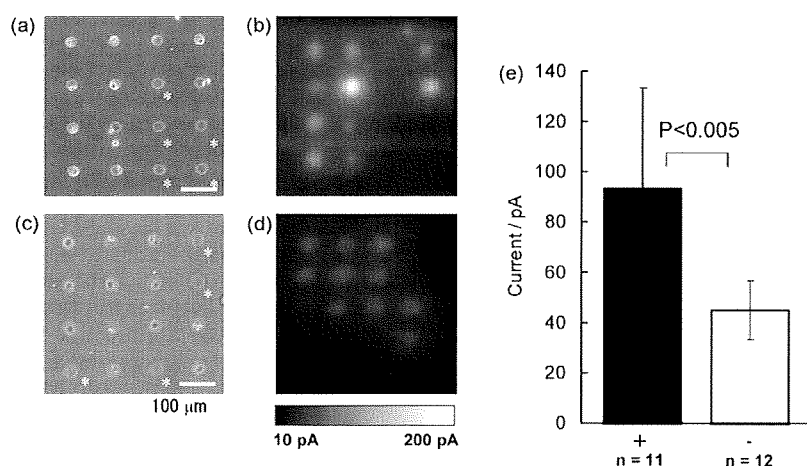


**Fig. 5.** The optical (a and c) and SECM images (b and d) of the single-cell array of HeLa-NFkB-SEAP cells with (a and b) and without (c and d)  $100 \text{ ng mL}^{-1}$  TNF- $\alpha$  stimulation on the PDMS stencil/polystyrene device not subjected to pDEP. The vacant well was marked as (\*). SECM was performed in the same conditions as those mentioned in Fig. 4. The SECM scan area was  $600 \mu\text{m} \times 600 \mu\text{m}$ . (e) The average current response of the HeLa-NFkB-SEAP cells with (filled bar,  $n = 11$ ) and without TNF- $\alpha$  stimulation (open bar,  $n = 12$ ).

tool, especially for the purpose to monitor cellular signal transduction pathway. Microwell array is appropriate to control the diffusion of reactants and products from single cells because the concentration profile near the microwell is defined by the geometry of the microwell rather than the original shape and size of the cell entrapped (Shiku et al., 2004). We found that wild-type HeLa has endogenous (natural) alkaline phosphatase activity. Current response due to topographic change in the microwell may be negligible because we confirmed that there was no current response for the polystyrene beads without alkaline phosphatase on the SU-8 microwell array/ITO s shown in Fig. S-5.

As shown above, SECM allows statistic analysis of electrochemical responses from single cells. Therefore, we next tried to monitor the signal transduction in the cells by switching on/off the expression of the reporter gene that was under the control of promoter region, and which was responsible for the binding of the transcription factors at the responsive elements in the DNA sequences. We selected the NF $\kappa$ B pathway as the model, in which the NF $\kappa$ B protein complex binds to the  $\kappa$ B element triggering transcription of the genes downstream of the promoter region. HeLa cells were transfected with a plasmid vector pNF $\kappa$ B-SEAP (HeLa-NF $\kappa$ B-SEAP) that secreted SEAP upon stimulation with TNF- $\alpha$ . Fig. 5 shows the optical and SECM images of the single-cell array of HeLa-NF $\kappa$ B-SEAP cells with and without TNF- $\alpha$  stimulation. The cells were arrayed in the PDMS microstencil/polystyrene without applying pDEP. Panels (a) and (b) were taken after the incubation with the RPMI medium for 5 h and with the RPMI medium containing 100 ng mL<sup>-1</sup> TNF- $\alpha$  for 2 h. Panels (c) and (d) were taken after the incubation with the RPMI medium for 8 h. The average current response of HeLa-NF $\kappa$ B-SEAP (filled bar,  $n = 11$ ) cells stimulated with TNF- $\alpha$  was significantly larger than that of the untreated cells (open bar,  $n = 12$ ) (Fig. 5e), indicating that TNF- $\alpha$  activates the intracellular signaling pathway for the production of SEAP.

In order to clarify the influence of pDEP, the HeLa-NF $\kappa$ B-SEAP cells that localized on the SU-8 microwell array/ITO in the form of a 4  $\times$  3 single-cell array after pDEP manipulation were subjected to SECM analysis. The SECM response in this case was very large even before stimulation with TNF- $\alpha$ . Moreover, this response was noted to increase during the 5-h culture, which promoted cell adhesion (Supplement, Fig S-6). This elevation of the background response was probably due to the stress by pDEP and/or the SU-8 material. Although almost all the cells were alive after DEP, it does not indicate that the pDEP manipulation is completely stress free. The SECM responses of the pDEP-manipulated single cells in the SU-8 microwell array/ITO were compared before and after TNF- $\alpha$  stimulation. The oxidation current responses of a single HeLa-NF $\kappa$ B-SEAP cell as determined by the single-scan mode SECM before and after TNF- $\alpha$  stimulation were  $51.04 \pm 14.42$  ( $n = 7$ ) and  $43.48 \pm 7.87$  pA ( $n = 8$ ), respectively. No significant difference was noted ( $p > 0.25$ ).

In our previous studies, we have reported the use of a novel electrochemical device comprising orthogonally positioned arrays of column- and row-electrodes for the analysis of single-cell gene expression (Lin et al., 2009). By using the electrode array device, PAP produced from a single cell was oxidized at the row-electrode set at 0.3 V vs. Ag/AgCl. The oxidized product, i.e., *p*-quinoneimine (QI) underwent reduction to form PAP at the column electrode set at 0.0 V vs. Ag/AgCl; 100 points of the cross section of the column- and row-electrodes were collected within 22 s. However, typically, it takes 25 min to capture a single SECM image (600  $\mu$ m  $\times$  450  $\mu$ m, 12 microchambers). Although SECM imaging is not as fast as electrochemical analysis using our device previously reported, the oxidation current of ca. 60 pA obtained for a single HeLa-SEAP cell in the microchamber by using SECM was significantly larger than that obtained by using the electrochemical device ( $16.3 \pm 5.49$  pA ( $n = 67$ )). This is because SECM estimates the PAP oxidation current from the upper side of the microwell with the simplest manner. The

current response of several tens of pA obtained by SECM made the statistic analysis more reliable, and consequently, we were successful in accomplishing the electrochemical monitoring of the signal transduction pathways at the single-cell level for the first time.

#### 4. Conclusion

In this study, the expression of SEAP was electrochemically monitored at the single-cell level by SECM. First, we constructed a single-cell array and subjected it to pDEP. The SECM response of HeLa cells that constitutively expressed SEAP (HeLa-pSEAP2-Control) was significantly large compared to that of the wild-type HeLa cells ( $p < 0.0001$ ). Next, we transfected the HeLa cells with a plasmid containing SEAP under the control of a responsive element ( $\kappa$ B element). The SECM measurements indicated that TNF- $\alpha$  stimulation remarkably increased the response of the transfected cells arrayed on the PDMS microstencil/polystyrene without subjecting them to pDEP. The average current responses of HeLa-NF $\kappa$ B-SEAP cells with and without TNF- $\alpha$  stimulation were significantly distinguishable ( $p < 0.005$ ). However, a very high SECM response was obtained even before the stimulation of cells with TNF- $\alpha$  during single-cell manipulation by pDEP on the SU-8 microwell array/ITO. Moreover, the response of the untreated cells increased during the 5-h culture that promoted cell adhesion. These results suggest that the stress caused by pDEP and/or the SU-8 material triggers intracellular signaling to produce SEAP.

#### Acknowledgements

This work was partly supported by Grants-in-Aid for Scientific Research (18101006, 21685008) from MEXT (Ministry of Education, Culture, Sports, Science and Technology), Japan; by a Grant-in-Aid for Scientific Research on Priority Areas (17066002) "Life Surveyor" from MEXT; and by a grant from the Center for Interdisciplinary Research, Tohoku University.

#### Appendix A. Supplementary data

Supplementary data associated with this article can be found, in the online version, at doi:10.1016/j.bios.2009.09.001.

#### References

- Bard, A.J., Fan, F.-R.F., Kwak, J., Lev, O., 1989. *Anal. Chem.* 61, 132–138.
- Bard, A.J., Li, X., Zhan, W., 2006. *Biosens. Bioelectron.* 22, 461–472.
- Chen, C.S., Mrksich, M., Huang, S., Whitesides, G.M., Ingber, D.E., 1997. *Science* 276, 425–428.
- Chang, C.-Y., Murata, T., Takahashi, Y., Shiku, H., Chang, H.-C., Matsue, T., 2009. *Lab. Chip* 9, 1185–1192.
- Daunert, S., Barrett, G., Feliciano, J.S., Shetty, R.S., Shrestha, S., Spencer, W.S., 2000. *Chem. Rev.* 100, 2705–2738.
- Di Carlo, D., Aghdam, N., Lee, L.P., 2006. *Anal. Chem.* 78, 4925–4930.
- Folch, A., Jo, B.H., Hurtado, O., Beebe, D.J., Toner, M., 2000. *J. Biomed. Mater. Res.* 52, 346–353.
- Gray, D.S., Tan, J.L., Voldman, J., Chen, C.S., 2004. *Biosens. Bioelectron.* 19, 771–780.
- Hosokawa, M., Arakaki, A., Takahashi, M., Mori, T., Takeyama, H., Matsunaga, T., 2009. *Anal. Chem.* 81, 5308–5313.
- Ino, K., Okochi, M., Konishi, N., Nakatochi, M., Imai, R., Shikida, M., Ito, A., Honda, A., 2008. *Lab. Chip* 8, 134–142.
- Kaff, B.M., Voldman, J., 2005. *Anal. Chem.* 77, 7976–7983.
- Kaya, T., Torisawa, Y.S., Oyamatsu, D., Nishizawa, M., Matsue, T., 2003. *Biosens. Bioelectron.* 18, 1379–1383.
- Kelso, E., McLean, J., Cardoso, M.F., 2000. *Electroanalysis* 12, 490–494.
- Kovac, J.R., Voldman, J., 2007. *Anal. Chem.* 79, 9321–9330.
- Kunikata, R., Takahashi, Y., Koide, M., Itayama, T., Yasukawa, T., Shiku, H., Matsue, T., 2009. *Sens. Actuators B* 141, 256–262.
- Lee, H.J., Yasukawa, T., Suzuki, M., Taki, Y., Tanaka, A., Kameyama, M., Shiku, H., Matsue, T., 2008. *Sens. Actuators B* 131, 424–431.
- Lee, H.J., Yasukawa, T., Suzuki, M., Lee, S.H., Yao, T., Taki, Y., Tanaka, A., Kameyama, M., Shiku, H., Matsue, T., 2009. *Sens. Actuators B* 136, 320–325. doi:10.1016/j.snb.2008.12.054.
- Li, X., Bard, A.J., 2009. *J. Electroanal. Chem.* 628, 35–42.

- Lin, Z., Takahashi, Y., Kitagawa, Y., Umemura, T., Shiku, H., Matsue, T., 2008. *Anal. Chem.* 80, 6830–6833.
- Lin, Z., Takahashi, Y., Murata, T., Takeda, M., Ino, K., Shiku, H., Matsue, T., 2009. *Angew. Chem. Int. Ed.* 48, 2044–2046.
- Matsue, T., Matsumoto, N., Koike, S., Uchida, I., 1993. *Biochim. Biophys. Acta—Gen. Subjects* 1157, 332–335.
- Matsue, T., Matsumoto, N., Uchida, I., 1997. *Electrochim. Acta* 42, 3251–3256.
- Matsumoto, N., Matsue, T., Uchida, I., 1994. *Bioelectrochem. Bioenergy* 34, 199–202.
- Matsunaga, T., Hosokawa, M., Arakaki, A., Taguchi, T., Mori, T., Tanaka, T., Takeyama, H., 2008. *Anal. Chem.* 80, 5139–5145.
- Mauzeroll, J., Bard, A.J., 2004. *Proc. Natl. Acad. Sci. U.S.A.* 101, 7862–7867.
- Neugebauer, S., Zimdars, A., Liepold, P., Gebala, M., Schuhmann, W., Hartwich, G., 2009. *Chem. Biol. Chem.* 10, 1193–1199.
- Nishizawa, M., Takoh, K., Matsue, T., 2002. *Langmuir* 18, 3645–3649.
- Retting, J.R., Folch, A., 2005. *Anal. Chem.* 77, 5628–5634.
- Roberts, W.S., Lonsdale, D.J., Griffiths, J., Higson, S.P.J., 2007. *Biosens. Bioelectron.* 23, 301–318.
- Sasuga, Y., Iwasa, T., Terada, K., Oe, Y., Sorimachi, H., Ohara, O., Harada, Y., 2008. *Anal. Chem.* 80, 9141–9149.
- Schrock, D.S., Baur, J.E., 2007. *Anal. Chem.* 79, 7053–7061.
- Schulte, A., Schuhmann, W., 2007. *Angew. Chem. Int. Ed.* 46, 2–20.
- Shiku, H., Takeda, M., Murata, T., Akiba, U., Hamada, F., Matsue, T., 2009. *Anal. Chim. Acta* 640, 87–92.
- Shiku, H., Shiraishi, T., Aoyagi, S., Utsumi, Y., Matsudaira, M., Abe, H., Hoshi, H., Kasai, S., Ohya, H., Matsue, T., 2004. *Anal. Chim. Acta* 522, 51–58.
- Sims, C.E., Allbritton, N.L., 2007. *Lab. Chip* 7, 423–440.
- Skelley, A.M., Kirak, O., Suh, H., Jaenisch, R., Voldman, J., 2009. *Nat. Methods* 6, 147–152.
- Suzuki, M., Yasukawa, T., Shiku, H., Matsue, T., 2008. *Biosens. Bioelectron.* 24, 1043–1047, doi:10.1016/j.bios.2008.06.051.
- Takahashi, Y., Hirano, Y., Yasukawa, T., Shiku, H., Yamada, H., Matsue, T., 2006. *Langmuir* 22, 10299–10306.
- Takahashi, Y., Miyamoto, T., Shiku, H., Asano, R., Yasukawa, T., Kumagai, I., Matsue, T., 2009. *Anal. Chem.* 81, 2785–2790.
- Torisawa, Y.S., Ohara, N., Nagamine, K., Kasai, S., Yasukawa, T., Shiku, H., Matsue, T., 2006. *Anal. Chem.* 78, 7625–7631.
- Torisawa, Y.S., Takagi, A., Nashimoto, Y., Yasukawa, T., Shiku, H., Matsue, T., 2007. *Biomaterials* 28, 559–566.
- Wittstock, G., Burchardt, M., Pust, S.E., Shen, Y., Zhao, C., 2007. *Angew. Chem. Int. Ed.* 46, 1584–1617.
- Whitaker, R.D., Walt, D.R., 2007. *Anal. Chem.* 79, 9045–9053.
- Yamamura, S., Kishi, H., Tokimitsu, Y., Kondo, S., Honda, R., Ramachandra Rao, S., Omori, M., Tamiya, E., Muraguchi, A., 2005. *Anal. Chem.* 77, 8050–8056.
- Yasukawa, T., Kondo, Y., Uchida, I., Matsue, T., 1998. *Chem. Lett.* 27, 767–768.
- Yasukawa, T., Nagamine, K., Horiguchi, Y., Shiku, H., Koide, M., Itayama, T., Shiraishi, F., Matsue, T., 2008. *Anal. Chem.* 80, 3722–3727.
- Zhou, H., Kasai, S., Noda, H., Ohya-Nishiguchi, H., Shiku, H., Matsue, T., 2003. *Bull. Chem. Soc. Jpn.* 76, 1757–1762.

## Hyaluronic acid reagent suppressed endometriotic lesion formation in a mouse model

In an animal endometriosis model, the administration of hyaluronic acid (HA) reagent significantly suppressed the formation of endometriotic lesions in both number and weight. This effect was found when HA treatment was conducted at the time of endometrial fragment inoculation. (Fertil Steril® 2010;93:2757–9. ©2010 by American Society for Reproductive Medicine.)

Endometriosis is an enigmatic disease that affects women of reproductive age, causing a decline in health, and has been associated with infertility (1). Implantation of endometrial tissues in retrograde menstrual flux is a widely accepted etiology of the disease. From this perspective, to study molecules which prevent implantation of endometrial tissues could be important not only to investigate the pathogenesis of endometriosis, but also to search for a new candidate for endometriosis treatment. But there is little knowledge about the mechanism of endometrial tissue implantation. In an earlier study using the *in vitro* adhesion model, hyaluronidase pretreatment of mesothelial cells decreased the binding of endometrial cells to mesothelium, indicating that hyaluronic acid (HA) plays a crucial role in the initiation of endometriosis (2). Interestingly, in the same study, there was no effect on endometrial cell binding to mesothelial cells when the endometrial cells were pretreated with hyaluronidase, suggesting that endometrial cells have a potential to bind to HA of surrounding tissue (2). Viewed inversely, saturating endometrial cells with exogenous HA may be a possible modality to prevent or reduce the formation of endo-

metriotic lesions. HA solution has the potential to serve this purpose, because it is already used clinically to prevent adhesion formation after abdominopelvic surgery (3). To investigate the hypothesis that exogenous HA might be a novel therapy for endometriosis, we studied the effect of HA solution on endometriosis in a mouse model.

Female 6–8-week-old BALB/c mice were used. All animal experiments were conducted according to the protocol approved by the Animal Care and Use Committee of the University of Tokyo. Induction of endometriosis was performed as previously described (4, 5). Briefly, ovariectomized mice were injected SC with 100 µg/kg estradiol valerate (Nihon Schering, Osaka, Japan) every week. Two weeks after ovariectomy, endometrium-rich fragments from donor mice were chopped using a razor blade. Fragments suspended in 0.6 mL phosphate-buffered saline (PBS) were injected with an 18-gauge needle through the abdominal wall into the peritoneal cavity of recipient mice with the ratio of one donor to two recipients (the day of endometrial fragment injection was designated day 0). The recipient mice underwent intraperitoneal injection of vehicle (PBS) or 100 µL HA (Chugai Pharmaceutical, Tokyo, Japan) once a week (days 0, 7, and 14; Fig. 1, Exp. 1). In some experiments, mice underwent the administration of HA either starting 1 week after the injection of endometrial fragments (days 7 and 14; Fig. 1, Exp. 2) or only at the time of injection of endometrial fragments (day 0; Fig. 1, Exp. 3). Three weeks after the injection of endometrial fragments (day 21), the mice were killed by cervical dislocation. Then PBS (0.8 mL) was injected into the peritoneal cavity. After vigorous shaking, peritoneal fluid was collected and the supernatant was kept at –80°C until assay. Laparotomy was performed, and the number of endometriotic foci was counted as previously described (4, 5). The interface between endometriotic foci and normal tissues appeared to be loose, and the foci, pulled by forceps, were easily resected. The weight of the excised tissues was then measured. In the case of cystic lesions, fluid contents were excluded before measurement. In all of the procedures, examiners were blinded to the treatment given to each mouse. Data are expressed as mean ± SEM. Mann-Whitney *U* test and Student *t* test for paired comparison were used. Statistical significance was defined as  $P < .05$ .

As we have reported, endometriotic lesions were observed as cystic lesions, and all were excised from the surrounding tissue

Akiko Hasegawa, M.D., Ph.D.<sup>a</sup>

Osamu Yoshino, M.D., Ph.D.<sup>a,b</sup>

Yutaka Osuga, M.D., Ph.D.<sup>a</sup>

Ako Kodama, M.D.<sup>a</sup>

Masashi Takamura, M.D.<sup>a</sup>

Osamu Nishii, M.D., Ph.D.<sup>b</sup>

Yuji Taketani, M.D., Ph.D.<sup>a</sup>

<sup>a</sup> Department of Obstetrics and Gynecology, University of Tokyo, Tokyo, Japan

<sup>b</sup> Department of Obstetrics and Gynecology, Mizonokuchi Hospital, Teikyo University, Kawasaki, Japan

Received June 30, 2009; revised and accepted February 23, 2010; published online March 31, 2010.

A.H. has nothing to disclose. O.Y. has nothing to disclose. Y.O. has nothing to disclose. A.K. has nothing to disclose. M.T. has nothing to disclose. O.N. has nothing to disclose. Y.T. has nothing to disclose.

Supported in part by Health and Labor Sciences research grants from the Ministry of Health, Labor and Welfare of Japan, grants from the Ministry of Education, Culture, Sports, Science and Technology, and by the Yamaguchi Endocrine Research Association.

Reprint requests: Osamu Yoshino, Department of Obstetrics and Gynecology, University of Tokyo, Tokyo 113-8655, Japan (FAX: 81-3-3816-2017; E-mail: oyoshino624@hotmail.co.jp).